Quantum correlations and entanglement in far-from-equilibrium spin systems

Kaden R. A. Hazzard,[1,*] Mauritz van den Worm,[2] Michael Foss-Feig,[3] Salvatore R. Manmana,[4] Emanuele G. Dalla Torre,[5]
Tilman Pfau,[6] Michael Kastner,[7,2] and Ana Maria Rey[1]

[1]*JILA and Department of Physics, University of Colorado-Boulder, NIST, Boulder, Colorado 80309-0440, USA*
[2]*Institute of Theoretical Physics, University of Stellenbosch, Stellenbosch 7600, South Africa*
[3]*JQI, NIST, Department of Physics, University of Maryland, College Park, Maryland 20742, USA*
[4]*Institute for Theoretical Physics, Georg-August-Universität Göttingen, D-37077 Göttingen, Germany*
[5]*Department of Physics, Harvard University, Cambridge, Massachusetts 01238, USA*
[6]*5. Physikalisches Institut and Center for Integrated Quantum Science and Technology,
Universität Stuttgart, Pfaffenwaldring 57, 70569 Stuttgart, Germany*
[7]*National Institute for Theoretical Physics (NITheP), Stellenbosch 7600, South Africa*

By applying complementary analytic and numerical methods, we investigate the dynamics of spin-$\frac{1}{2}$ XXZ models with variable-range interactions in arbitrary dimensions. The dynamics we consider is initiated from uncorrelated states that are easily prepared in experiments; it can be equivalently viewed as either Ramsey spectroscopy or a quantum quench. Our primary focus is the dynamical emergence of correlations and entanglement in these far-from-equilibrium interacting quantum systems: We characterize these correlations by the entanglement entropy, concurrence, and squeezing, which are inequivalent measures of entanglement corresponding to different quantum resources. In one spatial dimension, we show that the time evolution of correlation functions manifests a nonperturbative dynamic singularity. This singularity is characterized by a universal power-law exponent that is insensitive to small perturbations. Explicit realizations of these models in current experiments using polar molecules, trapped ions, Rydberg atoms, magnetic atoms, and alkaline-earth and alkali-metal atoms in optical lattices, along with the relative merits and limitations of these different systems, are discussed.

I. INTRODUCTION

Recent advances in ultracold atom, molecule, and ion experiments [1] and the development and application of ultrafast pulsed lasers to probe strongly correlated dynamics in solid-state systems [2] have enabled the experimental study of dynamics in far-from-equilibrium quantum many-body systems [1]. For example, an abrupt change of parameters in a system's Hamiltonian can create entangled states suitable for quantum metrology and information [3–5], enable one to investigate equilibration and thermalization [6,7], and be used to characterize fundamental quantum behavior. These experimental capabilities have, in turn, stimulated a large body of theoretical work, largely because the inherent complexity of far-from-equilibrium interacting quantum systems renders inapplicable most of the standard theoretical tools developed for equilibrium physics.

In this work we study the time evolution of spin-$\frac{1}{2}$ XXZ models following a quantum quench. We treat systems with varying—and often arbitrary—dimensionality and spatial structure of the couplings, including interactions that decay as a power law with distance, which recently have attracted much attention due to their importance in, for example, ultracold polar molecules [8,9], Rydberg atoms [10–15], magnetic atoms [16], and trapped ions [17,18]. For simplicity we focus most of our attention on initial states that are translationally invariant and uncorrelated product states, which can easily be created by subjecting an initially spin-polarized system to

a strong resonant pulse that initiates the quantum dynamics. The specific initialization protocol we consider and the spin models that we study are relevant to numerous ultracold atomic and molecular systems in which the motional degrees of freedom have been frozen out, including trapped ions [17,18], magnetic atoms [19–21], Rydberg atoms [10–15], ultracold polar molecules [8,9], and optical atomic clocks [22–25], as well as to condensed-matter systems ranging from nitrogen-vacancy centers in diamond [26] and other magnetic defects in solids [27] and to traditional quantum magnets where the spins are realized by electrons localized in a nuclear lattice [28–31]. A more comprehensive discussion of physical realizations is given in Sec. VII.

The main objective of this work is to characterize and understand the dynamics of local observables, correlations, and entanglement and their dependence on initial conditions (e.g., spin direction) and range of interactions. Various analytical and numerical techniques are employed, including short-time perturbative methods, exact solutions for the Ising model, and Luttinger liquid theory, together with numerically exact methods [32] for one-dimensional spin chains. We compute the von Neumann entanglement entropy, the concurrence, and the spin-squeezing parameter, each of which quantifies a distinct quantum correlation and resource. Spin squeezing, for example, quantifies the quantum correlations that are useful for enhanced metrology with sensitivity beyond that achievable with unentangled spins, referred to as the standard quantum limit.

An important issue addressed in this work is the strength of the correlations and of the entanglement obtained in the course of the time evolution. In general, we find that both correlations and entanglement become significantly larger

*kaden.hazzard@gmail.com

than they are in the corresponding ground state. Moreover, at long times, we find evidence that, although not maximal, the entanglement follows a volume law rather than an area law. Such results provide a strong contrast with classical dynamics. Although there is a large literature on the nonequilibrium dynamics of classical spin models (Refs. [37–42] contain recent reviews), which have some similarities to the quantum case (for example, exponential decay of a nonconserved quantity through local relaxation, as opposed global transport through diffusion), there are also many properties that are unique to the quantum dynamics. The entanglement measures furnish a strong example, since they all vanish at all times for classical systems. It would be interesting to explore more thoroughly the similarities and differences between classical and quantum dynamics, but such a comparison is beyond the scope of the present paper, especially given the rich variety of classical dynamical phenomena.

An important question regarding the growth of correlations in nonequilibrium systems is whether they exhibit universal behaviors and, if so, how that universality manifests. We show in a one-dimensional system that universality is realized as a dynamic power-law singularity appearing beyond any order of perturbation theory. The behavior is controlled by a universal power-law exponent; this exponent is universal in the sense that it is insensitive to small perturbations.

We also aim to provide a brief but fairly comprehensive overview of various experimental systems to which our results apply, highlighting their unique features and tabulating the form of the interactions, characteristic energy and time scales, and parameter regimes available to each system. Table I summarizes several of these and serves as a "dictionary" to translate results between systems.

The paper is organized as follows. Section II introduces the XXZ Hamiltonian and the quench protocol (equivalent to Ramsey spectroscopy) that we study, along with notation used throughou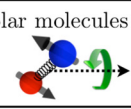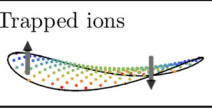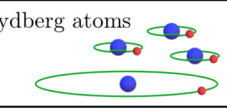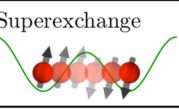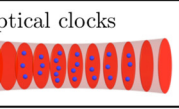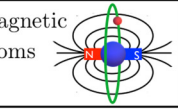t the rest of the text. Next we calculate the dynamics of correlation functions in the short-time limit (Sec. III) and the Ising limit (Sec. IV A) and discuss its physical interpretation. These calculations are primarily a review of prior work and are included mainly to be self-contained and set the context for calculations of entanglement and universality out of equilibrium (although they do contain some useful new results and rearrangements of prior results). Section IV B considers various entanglement measures for the Ising dynamics, including entanglement entropies for two-site "cutout" bipartitions, spin squeezing, and concurrence. Although entanglement is a rather generic feature, a quantitative analysis comparing the dynamics of these different entanglement measures in a general many-body setting has been lacking. We show that different types of entanglement, each corresponding to a different quantum resource, become dominant at different times of the Ising dynamics. Section V turns to entanglement in the more general XXZ dynamics in one-dimensional spin chains, where we apply the adaptive time-dependent density matrix renormalization group method (adaptive t-DMRG [33–36]). We quantify the strength of the entanglement emerging in the dynamics by comparing to the entanglement in the corresponding equilibrium systems as well as to maximally entangled states. In Sec. VI we demonstrate an explicit example of universal behavior out of equilibrium. Section VII summarizes the applicability and relevance of our finding to a variety of atomic, molecular, and optical systems, some of which is summarized in Table I. Finally, Sec. VIII concludes and presents an outlook on future theoretical and experimental work.

II. HAMILTONIAN AND NONEQUILIBRIUM DYNAMIC PROCEDURE

A. Hamiltonian

We consider the numerous physical systems in atomic and condensed-matter physics that are unified by their description

TABLE I. (Color online) Properties of several physical systems that can be used to realize the spin models and nonequilibrium dynamics considered in this paper. (a) *Spin-coupling.* Achievable spin couplings, reported as J_x, J_y, J_z, are to be understood as coefficients of the Hamiltonian $\mathcal{H} = (1/2) \sum_{i \neq j} (J_x S_i^x S_j^x + J_y S_i^y S_j^y + J_z S_i^z S_j^z)$. (b) *Spatial structure.* The distance and angular dependence of the interactions is presented. (c) *Coupling strengths.* Typical coupling strengths are given as a range (in Hertz), which is intended to reflect reasonable values realizable in current implementations of these systems. (d) *Coherence times.* Coherence times given are rough lower bounds, but in some special cases (for example, by using field-insensitive clock transitions in ions) these times can greatly exceed the stated values. (e) *Number of spins.* System sizes quoted reflect rough upper limits achieved in current experiments. Rydberg atoms exist in a wide variety of regimes, and the numbers given encompass many different experimental situations.

	Polar molecules	Trapped ions	Rydberg atoms	Superexchange	Optical clocks	Magnetic atoms
(a)	$J_\perp, J_\perp, J_z$	$J_\perp, J_\perp, 0$ or $0, 0, J_z$	$J_\perp, J_\perp, J_z$ or $0, 0, J_z$	$J_\perp, J_\perp, J_z$	$J_\perp, J_\perp, J_z$	$J_\perp, J_\perp, -2J_\perp$
(b)	$(1 - 3\cos^2\theta)/r^3$	$1/r^\alpha$; $0 < \alpha < 3$	$(1 - 3\cos^2\theta)/r^3$ or $1/r^6$	Nearest neighbor	Variable long-range	$(1 - 3\cos^2\theta)/r^3$
(c)	$10^3 \lesssim J \lesssim 10^5$	$10^2 \lesssim J \lesssim 10^4$	$10^4 \lesssim J \lesssim 10^9$	$1 \lesssim J \lesssim 10^2$	$1 \lesssim J \lesssim 10^2$	$10 \lesssim J \lesssim 10^3$
(d)	$\tau \gtrsim 10^{-2}$ s	$\tau \gtrsim 10^{-3}$ s	$\tau \gtrsim 10^{-6}$ s	$\tau \gtrsim 1$ s	$\tau \gtrsim 10^{-1}$ s	$\tau \gtrsim 10^{-1}$ s
(e)	$N \lesssim 10^5$	$N \lesssim 10^2$	$N \lesssim 10^6$	$N \lesssim 10^6$	$N \lesssim 10^4$	$N \lesssim 10^5$

in terms of a spin-$\frac{1}{2}$ XXZ model,

$$H = \frac{1}{2} \sum_{i \neq j} \left[J_{ij}^z S_i^z S_j^z + \frac{J_{ij}^\perp}{2} (S_i^+ S_j^- + S_i^- S_j^+) \right], \quad (1)$$

where the sum extends over all pairs of sites of an arbitrary lattice. By S_i^z and $S_i^\pm = S_i^x \pm i S_i^y$, we denote the usual spin-$\frac{1}{2}$ operators at site i ($S_i^{x,y,z}$ are $1/2$ times the Pauli operators $\sigma_i^{x,y,z}$). We refer to the first term in Eq. (1) as the "direct" or Ising term and the second as the "exchange," "flip-flop," or XX term. The XX terminology comes from rewriting $(1/2)(S_i^+ S_j^- + S_i^- S_j^+) = S_i^x S_j^x + S_i^y S_j^y$ and observing that there are two couplings with the same strength along the $\hat{x}$ and $\hat{y}$ spin directions. We refer to the case when the XX term vanishes as the Ising Hamiltonian and the case when the Ising term vanishes as the XX Hamiltonian. In the specific case where $J_{ij}^z = J_{ij}^\perp$, it is possible to rewrite the Hamiltonian as $H = (1/2) \sum_{i \neq j} J_{ij} \mathbf{S}_i \cdot \mathbf{S}_j$, where $\mathbf{S}_i \equiv (S_i^x, S_i^y, S_i^z)$, which we refer to as the Heisenberg Hamiltonian.

In our analysis we allow the couplings J_{ij}^z and $J_{ij}^\perp$ to take arbitrary values, and unless otherwise specified we do not assume regularity of the couplings constants, translational invariance, or any particular type of boundary conditions. We note, however, that many of the numerical results that we show for correlations and entanglement focus on systems with open boundary conditions, especially since these lower the computational cost when t-DMRG is employed.

We also allow the (i,j) dependence of the couplings to be different for the Ising and XX terms, including distance and angle dependence. Similar anisotropies have been considered in models describing orbital magnetism in solid-state materials [43–45]. They are also important in exactly solvable models harboring topological phases, such as the Kitaev honeycomb model [46] and the Yao-Kivelson model [47], and in models harboring symmetry-protected topological ground states [48]. Some of these models break the U(1) symmetry assumed here (arising from the identical strength of the $S_i^x S_j^x$ and $S_i^y S_j^y$ interactions and the absence of cross terms like $S_i^x S_j^y$). However, although the lack of total S^z conservation associated with the broken U(1) symmetry can have important implications in the dynamics, we nevertheless expect that several of the features calculated herein (e.g., long-distance correlations, entanglement, and nonequilibrium universality) are likely to persist in these cases as well. Spin-spin interactions involving three or more sites are also possible, but these are beyond the scope of the present work.

In many situations, it is useful to add to H single-spin Zeeman terms, given by

$$H_1 = -\sum_i \mathbf{B}_i \cdot \mathbf{S}_i, \quad (2)$$

where the $\mathbf{B}_i$ are local magnetic fields which can vary in space. In this paper, such fields are useful for the preparation of initial states for our time evolution, but we only consider dynamics for $\mathbf{B}_i = 0$.

To give some idea of the form of the couplings $J_{ij}^{(\perp,z)}$ and the physical systems in which these couplings can arise, we start by briefly describing five disparate physical realizations of Eq. (1), chosen to reflect the diversity of these systems:

ultracold molecules in optical lattices, trapped ions, Rydberg atoms, ultracold atoms in optical lattices, and ultracold magnetic atoms (see Table I). Section VII provides a more comprehensive review of realizations of Eq. (1), the physics behind them, and basic characteristics of each system. The following discussion is intended merely to provide context and is unnecessary for understanding the formal results presented in Secs. III–VI.

In *ultracold polar molecules* pinned in optical lattices, two rotational states can be used to form the spin-$\frac{1}{2}$ degree of freedom, and the spin-spin couplings are induced by dipolar interactions. The difference in dipole moments between the two states (which arises in the presence of an electric field) generates the Ising term, while transition dipole moments between the two rotational states (which can exist even in the absence of an electric field) give rise to the spin-exchange terms [49–56]. Unlike the nearest-neighbor interactions arising from superexchange, the dipolar interactions are long-ranged and anisotropic. For the choices of rotational states used so far in experiments [8,9] J_{ij}^z and $J_{ij}^\perp$ are both proportional to $(1 - 3 \cos^2 \Theta_{ij})/r_{ij}^3$, where r_{ij} is the distance between the dipoles and Θ_{ij} is the angle between the intermolecular axis and the quantization axis provided by the external field (electric or magnetic). More complicated spin-spin interaction anisotropies, which can even break the U(1) symmetry, can be generated by more general choices of rotational states and/or by microwave dressing [50,55–58]. Other implementations of spin models in polar molecules using hyperfine levels to encode the spin have also been proposed; for example, see Ref. [59] and references therein.

In one- and two-dimensional *crystals of trapped ions*, hyperfine states can realize a spin-$\frac{1}{2}$. By addressing the ions with a spin-dependent optical potential, the vibrations of the crystal mediate a long-range Ising interaction that can be approximately described by a spatial power law $J_{ij} \propto 1/r_{ij}^\alpha$, with $0 \leqslant \alpha < 3$, where r_{ij} is the distance between ions i and j [17,18,60–63]. To engineer an XX model, it suffices to add a strong transverse field that projects out the off-resonant terms in the Ising interactions that change the magnetization along the field quantization direction [64]. More general XXZ models can be implemented, for example, by using multiple spin-dependent optical potentials [65].

In *frozen Rydberg gases* the Ising-type Hamiltonian can be realized via the strong Rydberg-Rydberg van der Waals interaction [66]. Typical experiments are very fast and limited by the Rydberg lifetime, which, in turn, guarantees that motional degrees of freedom remain frozen even without an underlying lattice potential. To obtain an (anisotropic) $1/r^3$ first-order dipolar potential between resonant dipoles oscillating between neighboring Rydberg states, one can employ so-called Förster resonances. As only the size of the Rydberg atoms limits the dipole moment, the resulting interaction strength can be very large and scales in the dipolar case as n^4 with the principal quantum number n.

For *ultracold spin-$\frac{1}{2}$ atoms* loaded into optical lattices, spin models emerge in Mott-insulating states, in which on-site interactions much stronger than the tunneling pin the lattice filling (for a range of chemical potentials) to integer numbers of atoms per site. In these systems, two hyperfine states encode the spin-$\frac{1}{2}$ degree of freedom and superexchange

processes [67] lead to spin-spin interactions of the XXZ form in Eq. (1). In this implementation the J_{ij} couplings are restricted to nearest neighbors. For spin-independent lattices, fermions realize a Heisenberg model, while for bosons the spin model is XXZ and depends on the relative sizes of the three scattering lengths between the two spin states, $a_{\uparrow\uparrow}$, $a_{\downarrow\downarrow}$, and $a_{\uparrow\downarrow}$. More general XXZ models can be realized with spin-dependent lattices.

Spin-exchange interactions also occur in *magnetic atoms*, which therefore realize spin models when confined in optical lattices [68]. In this case the spin degree of freedom is encoded in atomic hyperfine states (and, in general, it is not restricted to be spin $\frac{1}{2}$). Although, in general, magnetic dipole interactions include magnetization-changing terms [68] not accounted for in an XXZ spin model, these terms can be energetically suppressed at high-enough magnetic field. The magnetization-conserving dipolar interactions remain resonant and implement an XXZ spin model. In recent experiments carried out with Cr atoms with effective spin $S = 3$, the corresponding spin Hamiltonian realizes $J^z = -2J^\perp$ [69].

B. Dynamic procedure

Figure 1 depicts the dynamic procedure considered in this paper. All spins are initially aligned (at time $t = 0$) along some direction $\hat{n}$, and then this initial state $|\Psi(0)\rangle = \bigotimes_i |\hat{n}\rangle_i$ evolves under the XXZ Hamiltonian (1) for a time t. Then one measures time-dependent expectation values of observables $\langle \mathcal{O}(t) \rangle$, where the expectation value is taken in the time-evolved state $e^{-iHt}|\Psi(0)\rangle$. Because the interaction Hamiltonian possesses a U(1) symmetry associated with
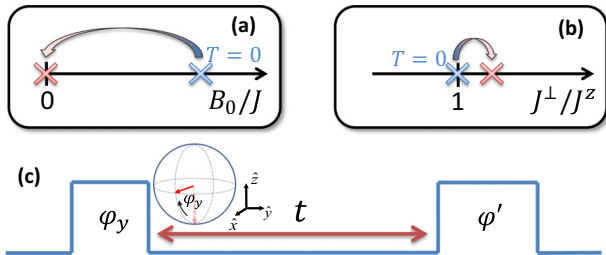

FIG. 1. (Color online) Three interpretations of the dynamic protocol that we study. (a) Sudden quench from the XXZ Hamiltonian with a strong magnetic field $B_0\hat{n}$ polarizing the spins in the $\hat{n}$ direction to zero field $B = 0$ for times $t > 0$, followed by a measurement of the observables at time t after the quench. (b) Sudden quench from the XXZ Hamiltonian at a ferromagnetic SU(2) symmetric point ($J_{ij}^z = J_{ij}^\perp$), where the ground states consist of all spins polarized along the same axis, to the XXZ Hamiltonian of interest. One adds an otherwise inconsequential infinitesimal magnetic field to choose the proper initial ground state. (In fact, this interpretation holds for antiferromagnetic interactions as well, since the dynamics is independent of multiplying the Hamiltonian by -1.) (c) Ramsey spectroscopy. Initial spins along the "down" ($-\hat{z}$) spin direction are rotated by an angle φ about the $\hat{y}$ spin direction. These evolve under the XXZ Hamiltonian (1) for an evolution time t. An arbitrary component of the Bloch vector can be read out by proper choice of the area (φ') and phase of the second pulse, and other correlation functions can be measured by high-resolution imaging and/or spin manipulation.

rotational invariance about the spin z axis, we can take the initial vector $\hat{n}$ to lie in the x-z plane, $\hat{n} = (\sin\varphi, 0, -\cos\varphi)$, without loss of generality. We refer to this angle φ as the "tipping angle."

This protocol has been used to observe dipolar spin-exchange interactions in ultracold molecules [8,9], to benchmark quantum simulators of hundreds of trapped ions [18], and to precisely measure atomic transitions as well as many-body interactions in optical lattice clocks [23,24,70,71]. Related protocols have been used or proposed for measuring spin relaxation, diffusion, and transport [72–81], for determining many-body interactions [8,13–15,18,24,82–86], for probing real-space correlations [87,88], and for characterizing topological order [89,90].

Despite the simplicity of this protocol, we see that the dynamics develops strong, long-ranged correlations, entanglement, and interesting dynamics that is frequently not captured by mean-field theory. Many of our results generalize to the case where the initial direction $\hat{n}$ can vary for each spin (some generalizations have been discussed in [91–93]), but here for simplicity we restrict our attention to uniform $\hat{n}$.

The dynamic protocol can be viewed either as Ramsey spectroscopy [illustrated in Fig. 1(c)] or as one of two different types of quantum quenches. From the perspective of Ramsey spectroscopy, the protocol begins by preparing all particles in the same internal state, which we consider to be the "spin-down" state. This preparation can typically be achieved with very high fidelity in ultracold atomic and molecular system, e.g., via optical pumping. An effective transverse field $B\sum_i S_i^y$ is then pulsed on for a time τ chosen to rotate each spin to the desired state $\hat{n}$ in the x-z plane by an angle $\varphi = B\tau$. This rotation requires that $B \gg \{J_{ij}^z, J_{ij}^\perp\}$ (and thus, for a fixed φ, that $\{J_{ij}^z\tau, J_{ij}^\perp\tau\} \ll 1$), so that we may neglect interactions during the pulse. After evolving for a time t under the interaction Hamiltonian, a final pulse rotates a desired Bloch-vector component onto the z axis, where it can be measured. The experimental appeal of the dynamic protocol considered in this paper is now evident: While cooling to ground states of interacting spin Hamiltonians can be extremely challenging in atomic and molecular systems, the preparation of each individual spin in its "down" state and the application of a pulsed effective transverse magnetic field is straightforward.

From the perspective of a quantum quench, the system starts in the ground state of an initial Hamiltonian (discussed below), the Hamiltonian is then suddenly switched to the XXZ Hamiltonian in Eq. (1), and the state is allowed to evolve for a time t before being measured. The first quench interpretation [illustrated in Fig. 1(a)] follows by considering the initial state to be the ground state of the Hamiltonian $H + H_1$, with $\mathbf{B}_i = B_0\hat{n}$, in a large ($B_0 \gg J^z, J^\perp$) magnetic field along the $\hat{n}$ direction, i.e., the ground state of H_1. The dynamics is then induced by suddenly turning off the magnetic field (from H_1) at time $t = 0$, leaving only the XXZ Hamiltonian H in Eq. (1). The second quench interpretation [illustrated in Fig. 1(b)] is to consider the initial state as the ground state of an initial Heisenberg Hamiltonian: $J_{ij}^z = J_{ij}^\perp < 0$ [94]. The states can be massively degenerate for large systems, corresponding to different directions in which the spins align. To break this potential degeneracy and choose the desired initial state with

all spins along $\hat{n}$, we can add a field $\mathbf{B}_i = \epsilon \hat{n}$ for an infinitesimal $\epsilon = 0^+$. In this way we can view the quench as being from the ground state of an initial SU(2) invariant Hamiltonian with $J_{ij}^z = J_{ij}^\perp$ to the more general XXZ Hamiltonian in Eq. (1). This perspective is particularly useful when Eq. (1) has $J_{ij}^z \approx J_{ij}^\perp$, such that the quench can be viewed as a small change in the Hamiltonian parameters. This is relevant to the emergence of universality out of equilibrium studied in Sec. VI. The sign of the overall Hamiltonian is irrelevant for the dynamics of many interesting observables, such as $\langle S^x(t) \rangle$. Therefore, when calculating such observables, the quench can be regarded as a perturbation if $J_{ij}^z \approx J_{ij}^\perp$, regardless of the overall sign of the couplings.

Before turning to our results, we emphasize that the Hamiltonian (1) is time independent. (Although the Ramsey spectroscopy's preparation and readout may be viewed as a time-dependent H_1 applied before and after the dynamics of interest.) Further interesting features may arise by considering dynamic coefficients, but they are beyond the scope of this paper.

III. SHORT-TIME RESULTS

For short times satisfying $\{J_{ij}^\perp t, J_{ij}^z t\} \ll 1$ (we set $\hbar = 1$ throughout), one can calculate correlation functions using time-dependent perturbation theory. The expectation value of an operator $\mathcal{O}$ evolves in time under a time-independent Hamiltonian H as $\langle \mathcal{O}(t) \rangle = \langle \mathcal{O} \rangle - it\langle[\mathcal{O},H]\rangle - \frac{t^2}{2}\langle[[\mathcal{O},H],H]\rangle + O(t^3)$, where the expectation value is taken in the initial state. We can evaluate these commutators and expectation values for the dynamics of interest, at least for low orders of perturbation theory.

Defining

$$\mathcal{C}_{ij}^{ab} \equiv \langle S_i^a S_j^b \rangle, \tag{3}$$

with $a,b \in \{x,y,z,+,-\}$, for $i \neq j$ we find

$$\langle S_i^x \rangle = \frac{1}{2}\sin\varphi\left\{1 - \frac{t^2}{8}\left[\Xi_i^{(2)}\sin^2\varphi + \left(\Xi_i^{(1)}\right)^2\cos^2\varphi\right]\right\} + O(t^4),$$

$$\langle S_i^y \rangle = -\frac{1}{2}\sin\varphi\left\{\frac{t}{2}\Xi_i^{(1)}\cos(\varphi)\right\} + O(t^3),$$

$$\mathcal{C}_{ij}^{xy} = \frac{t\sin(2\varphi)\sin\varphi}{16}\left[\left(J_{ij}^z - J_{ij}^\perp\right) - \Xi_j^{(1)}\right] + O(t^2),$$

$$\mathcal{C}_{ij}^{yz} = \frac{t}{8}\left[\frac{\sin(2\varphi)\cos\varphi}{2}\Xi_i^{(1)} + \left(J_{ij}^z - J_{ij}^\perp\right)\sin^3\varphi\right] + O(t^2),$$

$$\tag{4}$$

where we have defined

$$\Xi_i^{(m)} = \sum_{j \neq i}\left(J_{ij}^z - J_{ij}^\perp\right)^m. \tag{5}$$

The total z axis magnetization is conserved for all times: $\sum_i\langle S_i^z\rangle(t) = -(N/2)\cos\varphi$ for N spins. The correlators not shown (and those not trivially related to the shown correlators above by transposing the indices) are given by their $t = 0$ values to linear order. These results hold for arbitrary couplings

$J_{ij}^{\{z,\perp\}}$ and thus are valid for arbitrary dimensionality and boundary conditions, and with or without disorder.

Interestingly, the results given in Eq. (4) depend only on $J^\perp - J^z$. At quadratic order and higher order, however, general observables can depend on other parameters, such as $[(J^\perp)^2 - (J^z)^2]t^2$. The results for the case $J_{ij}^\perp = \lambda J_{ij}^z$ and assuming translational invariance were given in Ref. [95], which focused on dipolar interactions $J_{ij}^z \propto (1 - 3\cos^2\Theta_{ij})/r_{ij}^3$, with Θ_{ij} the angle between a quantization axis and the interparticle separation. The more general results given by Eq. (4) are useful for finite or disordered systems and for compass-type models where the spatial anisotropy and position-dependence may be different for the Ising and spin-exchange terms [43–46,48,57,58].

The connected correlation functions

$$\mathcal{G}_{ij}^{ab} \equiv \langle S_i^a S_j^b \rangle - \langle S_i^a \rangle\langle S_j^b \rangle \tag{6}$$

immediately follow from the results in Eq. (4),

$$\mathcal{G}_{ij}^{xy} = \frac{t\sin(2\varphi)\sin\varphi}{16}\left(J_{ij}^z - J_{ij}^\perp\right) + O(t^2),$$

$$\mathcal{G}_{ij}^{yz} = \frac{t\sin^3\varphi}{8}\left(J_{ij}^z - J_{ij}^\perp\right) + O(t^2). \tag{7}$$

The single-spin expectation values and correlation functions calculated here are directly accessible in experiments. For example, $\mathcal{C}_{ij}^{ab}$, which will be crucial input for the entanglement measures considered below, can be measured by high-resolution imaging or related to scattering results. These short-time expressions provide insight into the many-body dynamics. For example, one can see two distinct contributions to $\langle S_i^x \rangle$: a decrease due to precession, proportional to $\cos^2\varphi$, and a decrease associated with a shrinking Bloch-vector length of that spin due to entanglement with the other spins, proportional to $\sin^2\varphi$. The former can be understood within mean-field theory, while the latter is due to quantum fluctuations and cannot. The tipping angle dependence also suggests the parameter regime in which a mean-field description of the Bloch-vector dynamics is valid: For small tipping angles, $0 < \varphi \ll \pi/2$, mean-field effects dominate the dynamics, while as φ approaches $\pi/2$ the dynamics is dominated by genuine many-body correlations. The short-time formulas are also useful for estimating the convergence of new approximate theories, such as the "moving average cluster expansion" developed in Ref. [9].

IV. ISING LIMIT CORRELATIONS AND ENTANGLEMENT

A. Review of correlations in the Ising limit

Here we give an overview of the Bloch vector and correlation function dynamics in the Ising limit ($J_\perp = 0$). These observables are the basis for the computation of the entanglement entropy discussed in Sec. IV B. We also make use of the Ising correlation functions in Sec. V when comparing them to numerical results for the XXZ model in one dimension. There we discuss which features are particular to the Ising model and which generalize to the XXZ model.

While the equilibrium properties of the Ising model are classical, this is not the case for its dynamical properties, and mean-field theory fails to capture the dynamics in many

regimes. For example, for an initial $\varphi = \pi/2$ tipping angle, mean-field theory predicts that there is no dynamics, while, in fact, evolution occurs on a time scale set by J^z. Furthermore, starting from a product state the dynamics generates entangled states, including cluster states that suffice for one-way quantum computation [5], spin-squeezed states enabling quantum metrology [3,95], and Greenberger-Horne-Zeilinger (GHZ) states [4,96], a type of Schrödinger cat state. Nevertheless, the Ising limit does possess a special structure that facilitates the exact calculation of arbitrary-order correlation functions [91–93] and leads to unique dynamical features. In this work, we focus on the single-spin and two-spin expectation values, presented below.

In the Ising limit $J_\perp = 0$, the XXZ Hamiltonian (1) reduces to

$$H_{\text{Ising}} = \frac{1}{2} \sum_{i \neq j} J_{ij}^z S_i^z S_j^z. \qquad (8)$$

Note that we still consider completely arbitrary couplings $J^{\{z,\perp\}}$ and therefore arbitrary boundary conditions. Because all of the terms in this sum commute with one another, the time-evolution operator $U = e^{-iH_{\text{Ising}}t}$ factorizes, rendering analytic calculations possible [97–100]. Exact results have been derived for correlation functions of the Ising Hamiltonian (8) with arbitrary pure product initial states, even in the presence of general Markovian decoherence mechanisms [91,92], and for the coherent evolution of initial mixed product states [93]. Here we limit our calculations to initial states of the form

$$|\Psi(0)\rangle = \bigotimes_j \left(e^{i\phi_j/2} \cos\frac{\theta_j}{2} |\uparrow\rangle_j + e^{-i\phi_j/2} \sin\frac{\theta_j}{2} |\downarrow\rangle_j \right),$$
$$(9)$$

where θ_j and ϕ_j are the polar and azimuthal angles in the Bloch sphere representation, and $|\uparrow\rangle_j$ and $|\downarrow\rangle_j$ are eigenstates of S_j^z with eigenvalues $+1/2$ and $-1/2$, respectively.

Since S_j^z commutes with H_{Ising}, its expectation value remains constant during the time evolution,

$$\langle S_j^z \rangle(t) = \frac{1}{2} \cos\theta_j,$$
$$\mathcal{C}_{jk}^{zz}(t) = \frac{1}{4} \cos\theta_j \cos\theta_k. \qquad (10)$$

The expectation value of $S_j^\pm = S_j^x \pm i S_j^y$ is

$$\langle S_j^+ \rangle(t) = \frac{1}{2} e^{i\phi_j} \sin\theta_j \prod_{k \neq j} g_k^+(J_{kj}t), \qquad (11)$$

where

$$g_j^\pm(x) \equiv \cos^2(\theta_j/2) e^{-ix/2} \pm \sin^2(\theta_j/2) e^{ix/2}, \qquad (12)$$

and the x and y spin components are then given by

$$\langle S_j^x \rangle = \text{Re}\langle S_j^+ \rangle, \quad \langle S_j^y \rangle = \text{Im}\langle S_j^+ \rangle. \qquad (13)$$

The remaining two-point correlation functions are given by

$$\mathcal{C}_{jk}^{+z}(t) = \frac{1}{4} e^{i\phi_j} \sin\theta_j g_k^-(J_{jk}t) \prod_{l \neq j,k} g_l^+(J_{jl}t), \qquad (14)$$

$$\mathcal{C}_{jk}^{++}(t) = \frac{1}{4} e^{i(\phi_j+\phi_k)} \sin\theta_j \sin\theta_k \prod_{l \neq j,k} g_l^+(J_{jl}t + J_{kl}t), \qquad (15)$$

$$\mathcal{C}_{jk}^{+-}(t) = \frac{1}{4} e^{i(\phi_j-\phi_k)} \sin\theta_j \sin\theta_k \prod_{l \neq j,k} g_l^+(J_{jl}t - J_{kl}t). \qquad (16)$$

From the definitions, it follows that $\mathcal{C}_{jk}^{+-}(t) = \mathcal{C}_{jk}^{-+}(t)^*$, $\mathcal{C}_{jk}^{++}(t) = \mathcal{C}_{jk}^{--}(t)^*$, and $\mathcal{C}_{jk}^{+z}(t) = \mathcal{C}_{jk}^{-z}(t)^*$, and the x and y components of the spin correlators are given by

$$\mathcal{C}_{ij}^{xx} = \frac{1}{4}(\mathcal{C}_{ij}^{++} + \mathcal{C}_{ij}^{--} + \mathcal{C}_{ij}^{+-} + \mathcal{C}_{ij}^{-+}), \qquad (17)$$

$$\mathcal{C}_{ij}^{yy} = \frac{1}{4}(\mathcal{C}_{ij}^{+-} + \mathcal{C}_{ij}^{-+} - \mathcal{C}_{ij}^{++} - \mathcal{C}_{ij}^{--}), \qquad (18)$$

$$\mathcal{C}_{ij}^{xy} = \frac{1}{4i}(\mathcal{C}_{ij}^{++} - \mathcal{C}_{ij}^{--} - \mathcal{C}_{ij}^{+-} + \mathcal{C}_{ij}^{-+}). \qquad (19)$$

The connected correlators $\mathcal{G}_{ij}^{ab}$ follow from the expressions above. One finds

$$\mathcal{G}_{jk}^{+z} = \frac{e^{i\phi_j}}{4} \sin\theta_j \prod_{l \neq j,k} g_l^+(J_{jl}t)$$
$$\times [g_k^-(J_{jk}t) - \cos\theta_j g_k^+(J_{jk}t)], \qquad (20)$$

$$\mathcal{G}_{jk}^{++} = \frac{e^{i(\phi_j+\phi_k)}}{4} \sin\theta_j \sin\theta_k \Bigg[\prod_{l \neq j,k} g_l^+(J_{jl}t + J_{lk}t)$$
$$- g_k^+(J_{jk}t) g_j^+(J_{jk}t) \prod_{l \neq j,k} g_l^+(J_{jl}t) g_l^+(J_{lk}t) \Bigg], \qquad (21)$$

$$\mathcal{G}_{jk}^{+-} = \frac{e^{i(\phi_j-\phi_k)}}{4} \sin\theta_j \sin\theta_k \Bigg[\prod_{l \neq j,k} g_l^+(J_{jl}t - J_{lk}t)$$
$$- g_k^+(J_{jk}t) g_j^+(-J_{jk}t) \prod_{l \neq j,k} g_l^+(J_{jl}t) g_l^+(-J_{lk}t) \Bigg].$$
$$(22)$$

All higher-order correlation functions of $S^\pm$ and S^z involving more than two spins, such as $\langle S_i^a S_j^b S_k^c \rangle$ with $\{a,b,c\} \in \{\pm,z\}$, have simple exact expressions as well (see, for example, Refs. [91–93]), but we omit them here because they are unnecessary for our purposes.

B. Entanglement in the Ising limit

In this section we calculate and compare the dynamics of distinct entanglement measures in the Ising limit. Each measure quantifies a distinct quantum correlation and resource [101], and they help to classify and understand the structure of many-body phases of matter and dynamics [102].

An example of the qualitatively different dynamics of these distinct entanglement measures is furnished by the well-understood all-to-all coupling limit, $J_{ij} = J$ for all i and j, where Eq. (8) is known as the one-axis twisting Hamiltonian [3]. For an initial tipping angle $\varphi = \pi/2$, spin squeezing (one type of entanglement) emerges in this model at short times [3], while at later times an entangled GHZ state is generated (more discussion and definitions are given below) [103]. A spin-squeezed state exhibits enhanced phase sensitivity with respect to the shot noise limit in standard

Ramsey spectroscopy measurements but under Ising dynamics never reaches the Heisenberg limit (the maximum sensitivity allowed by quantum mechanics). In contrast, a GHZ state can reach the Heisenberg limit but, utilizing it in spectroscopy requires a modified Ramsey sequence, with a final readout based, for example, on spin-parity measurements $(-1)^{2S^z}$ [4].

Away from the all-to-all limit, the dynamics is much less well understood; calculating and understanding it are the main focuses of this section. For illustrative purposes, the coupling constants in Eq. (1) are chosen to be $J_{ij}^z = J/r_{ij}^\alpha$, where r_{ij} denotes the distance between spins i and j. For simplicity we consider one-dimensional lattices (i.e., chains), but our qualitative conclusions do not depend on this. We study the dependence of different entanglement measures on the initial tipping angle ($\phi_j = 0$ and $\theta_j = -\varphi$) and the range of interactions (α). We note that Ref. [104] has explored the α-dependence of the entanglement entropy dynamics in the related *transverse field* Ising model in one dimension.

Spin squeezing. Spin squeezing, which was introduced for the first time in Ref. [3], characterizes the sensitivity of a state to SU(2) rotations and is relevant for both entanglement detection (it is an entanglement witness) and quantum metrology (see Refs. [105,106] for more complete reviews). It also provides a lower bound on the minimum size of a genuine many-body entangled subsystem [107]. Spin-squeezed states can be visualized as states with anisotropic fluctuations of the spin vector in the directions perpendicular to the mean spin. Roughly speaking, a quantum state is considered spin squeezed if the variance of one spin component is smaller than that of an uncorrelated spin-coherent state. Due to the Heisenberg uncertainty relation, reduction of the variance in one direction causes an increase of fluctuations in the other. Spin squeezing is relatively easy to visualize, generate, and measure experimentally since it only involves the first and second moments of the collective angular momentum operators. We note that there are "generalized spin squeezing" entanglement witnesses that also depend only on the first and second moments of collective angular momentum operators [108,109], but to harness the associated entanglement requires more sophisticated protocols than the usual Ramsey spectroscopy.

There are multiple definitions of spin squeezing, depending on the context where it is used. Here we adopt the squeezing parameter introduced by Wineland *et al.* in the context of Ramsey spectroscopy [105],

$$\xi = \min_{\hat{n}} \frac{\sqrt{N}\sqrt{\langle (\mathbf{S} \cdot \hat{n})^2 \rangle - \langle \mathbf{S} \cdot \hat{n} \rangle^2}}{|\langle \mathbf{S} \rangle|}, \qquad (23)$$

where the minimization is over unit vectors $\hat{n}$ perpendicular to the mean spin direction $\langle \sum_i \mathbf{S}_i \rangle$. The correlation functions in the definition of ξ are readily evaluated using Eqs. (14)–(16) of the previous section. A state is then said to be squeezed when $\xi < 1$. It is common to report squeezing in decibels,

$$\text{dB squeezing} = -10 \log_{10} \xi^2, \qquad (24)$$

such that a state is squeezed when dB squeezing is positive. We note that squeezing is an entanglement witness for general mixed states: When dB squeezing is positive, the state is necessarily entangled [106,110,111].

In Ref. [3] the generation of spin squeezing was discussed for the case of a one-axis twisting (OAT) Hamiltonian $H_{\text{OAT}} = J(S^z)^2/2$, corresponding to the $\alpha = 0$ case of the Ising Hamiltonian Eq. (8). The OAT Hamiltonian generates spin-squeezed states at short times, a fact that has been confirmed in a number of experiments [112,113], but the squeezing is transient and disappears at longer times. However, the loss of spin squeezing does not necessarily imply a loss of entanglement; for example, at longer times ($t = \pi/J$) entangled GHZ states occur [103].

Figure 2(a) shows a contour plot of dB squeezing in the (α,t) plane, starting from a state that is fully polarized along the x spin direction ($\varphi = \pi/2, \phi = 0$). Increasing α leads to a slower and weaker creation of entanglement, but at the same time to a longer lifetime of the squeezed state. While there is a strong dependence of the spin squeezing on α for $\alpha < d$, where d is the dimension of the system, the dependence becomes weaker for $\alpha > d$.

Figure 2(d) shows dB spin squeezing in the (φ,t) plane for $\alpha = 3/4$. Maximal spin squeezing occurs for a tipping angle $\varphi = \pi/2$, implying that a fully x-polarized initial state (or any fully polarized state in the x-y plane) is the ideal choice for creating squeezed states under time evolution. As the tipping angle is decreased to around $\varphi = \pi/4$, spin squeezing persists and develops on a similar time scale to the $\varphi = \pi/2$ case, but reaches a smaller maximum value and disappears more quickly. This can be understood by noting that correlations $\mathcal{C}_{ij}^{az}$ containing a z component build up quickly and reduce spin squeezing, as illustrated in Fig. 3. As $\varphi \to 0$, the squeezing approaches zero, and the time at which the small amount of squeezing is created increases.

Entanglement entropy. The entanglement entropy between a subregion $\mathcal{R}$ and the rest of the system is given by

$$S_{\mathcal{R}} = -\text{Tr}\left(\rho_{\mathcal{R}} \ln \rho_{\mathcal{R}}\right), \qquad (25)$$

where $\rho_{\mathcal{R}}$ is the reduced density matrix of the subregion $\mathcal{R}$, obtained by tracing out all those parts of the Hilbert space not associated with $\mathcal{R}$. The entanglement entropy is a measure of the total entanglement of bipartite pure states (although even unentangled mixed states can have finite entanglement entropy) and is widely used in quantum information theory.

We consider subregions $\mathcal{R}_{ij} \equiv \{i,j\}$, consisting of pairs of (not necessarily neighboring) spins i and j. The reduced density matrix is given by

$$\rho_{\mathcal{R}_{ij}} = 4 \sum_{a,b \in \{0,x,y,z\}} \langle S_i^a S_j^b \rangle S_i^a S_j^b, \qquad (26)$$

with the convention that $2S_i^0$ is the 2×2 identity matrix at lattice site i. From this expression it becomes obvious that the results for the one- and two-spin correlation functions in Sec. IV allow us to also obtain exact results for the entanglement entropy of subregions $\mathcal{R}_{ij}$.

Figures 2(b) and 2(e) show $S_{\mathcal{R}_{ij}}$, where we have chosen $\mathcal{R}_{ij}$ as consisting of the sites adjacent (one to the left and one to the right) to the center spin of a chain with 41 sites. Entanglement monotonically decreases for tipping angles away from $\varphi = \pi/2$. This may be understood by considering that if we increase the tipping angle away from the fully x-polarized state, we increase the z component of the spin.
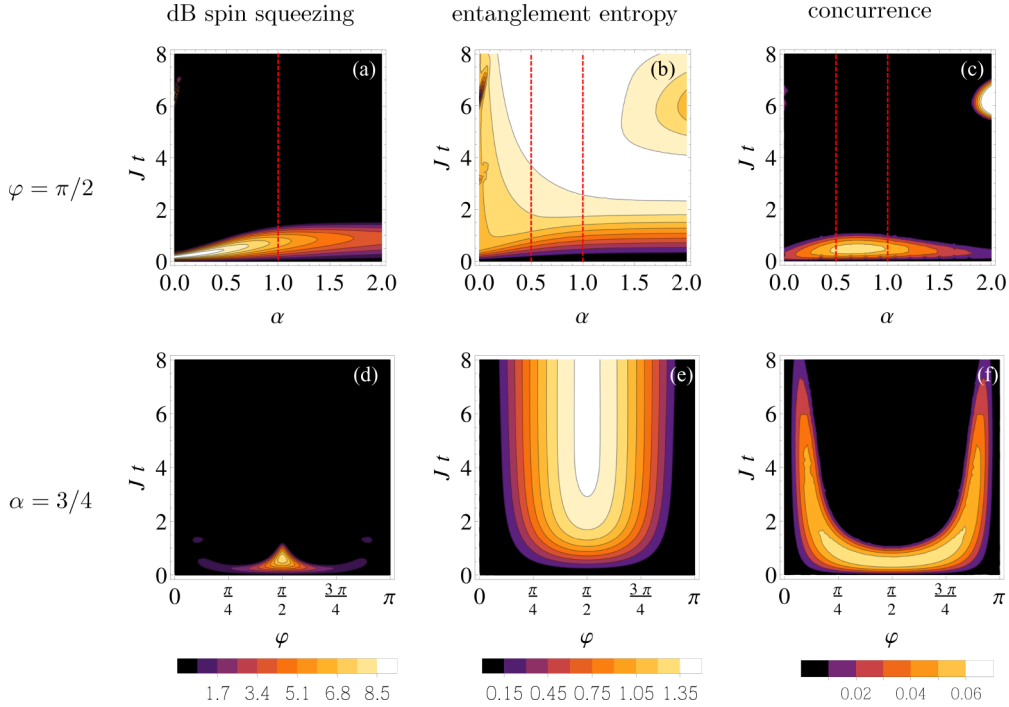
FIG. 2. (Color online) Time evolution of three entanglement measures for Ising chains with $L = 41$ lattice sites. (Top row) dB spin squeezing (left), entanglement entropy $S_{\mathcal{R}_{ij}}$ (middle), and concurrence (right) in the (α, t) plane, starting from a fully x-polarized $\varphi = \pi/2$ initial state. (Bottom row) As above, but in the (φ, t) plane for an interaction exponent $\alpha = 3/4$. The region $\mathcal{R}_{ij}$ is chosen to consist of next-nearest-neighbor spins at the center of the system. The same qualitative features are seen for alternative lattice geometries and for values of i and j that are not necessarily adjacent and at the center of the system. Vertical dashed red lines indicate $\alpha = d$ and $\alpha = d/2$, values where the character of the dynamics changes as discussed in the text.

Since components pointing along the z axis are conserved under the Ising time evolution, they will not contribute to the formation of entanglement. Hence, as we move the tipping angle away from the fully x-polarized state at $\varphi = \pi/2$, we expect the entanglement entropy to saturate at a lower value.

Figure 2(b) shows a contour plot of the entanglement entropy in the (α, t) plane. The entanglement entropy evolution shows differences depending on whether α is less or greater than $d/2$. For α substantially less than $d/2$ two well-separated time scales are apparent. On the shorter time scale (e.g., around $J^z t \approx 0.5$ for $\alpha = 0.1$) a quasistationary state [93] of intermediate entanglement strength is formed, while larger entanglement is built up on the longer time scale (around

$J^z t \approx 3$). The separation of scales is enhanced when increasing the number of lattice sites or by further reducing α. For $\alpha > d/2$ no such separation of time scales is visible; i.e., the aforementioned plateau is not apparent. When $\alpha > d$ the single- and two-spin correlation functions begin to show oscillatory behavior [see Fig. 4(a)]. These oscillations become more pronounced for greater values of α and can also be observed in the (α, t) plane for $\alpha \gtrsim 1.5$. Linear and Renyi entanglement entropies can also be computed from Sec. IV's correlation functions. The results obtained are qualitatively similar to those for the von Neumann entanglement entropy and are not shown here.

Concurrence. Concurrence was introduced in Ref. [114] as an entanglement measure for two-qubit systems that is valid for mixed states. It is defined as

$$\mathcal{C}(\rho) \equiv \max \{0, \lambda_1 - \lambda_2 - \lambda_3 - \lambda_4\}, \quad (27)$$

where $\lambda_1, \ldots, \lambda_4$ are the square roots of eigenvalues (in decreasing order) of the non-Hermitian matrix $\rho_{\mathcal{R}_{ij}} \sigma_i^y \sigma_j^y \rho_{\mathcal{R}_{ij}}^* \sigma_i^y \sigma_j^y$. Concurrence is an entanglement measure valid for mixed states (whereas, for example, entanglement entropy is an entanglement measure only for pure states), and its dynamics has recently been measured in trapped ion experiments [115].

While $\mathcal{S}_{\mathcal{R}_{ij}}$ measures the amount of entanglement between $\mathcal{R}_{ij}$ and the rest of the system (in the present case of a pure quantum state) [116], the concurrence measures the amount of entanglement *between* sites i and j. Figure 2(c) shows a contour plot of the concurrence in the (α, t) plane for a fully
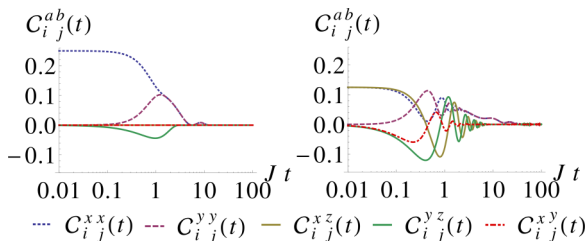

FIG. 3. (Color online) Time evolution of the two-spin correlation functions $\mathcal{C}_{ij}^{xx}(t)$, $\mathcal{C}_{ij}^{yy}(t)$, $\mathcal{C}_{ij}^{xy}(t)$, $\mathcal{C}_{ij}^{xz}(t)$, and $\mathcal{C}_{ij}^{yz}(t)$ for a power-law interacting Ising chain consisting of 41 lattice sites. The interaction exponent is $\alpha = 3/4$, with initial tipping angles $\varphi = \pi/2$ (left) and $\varphi = \pi/4$ (right). Lattice sites i and j are chosen one lattice spacing to either side of the center of the chain.
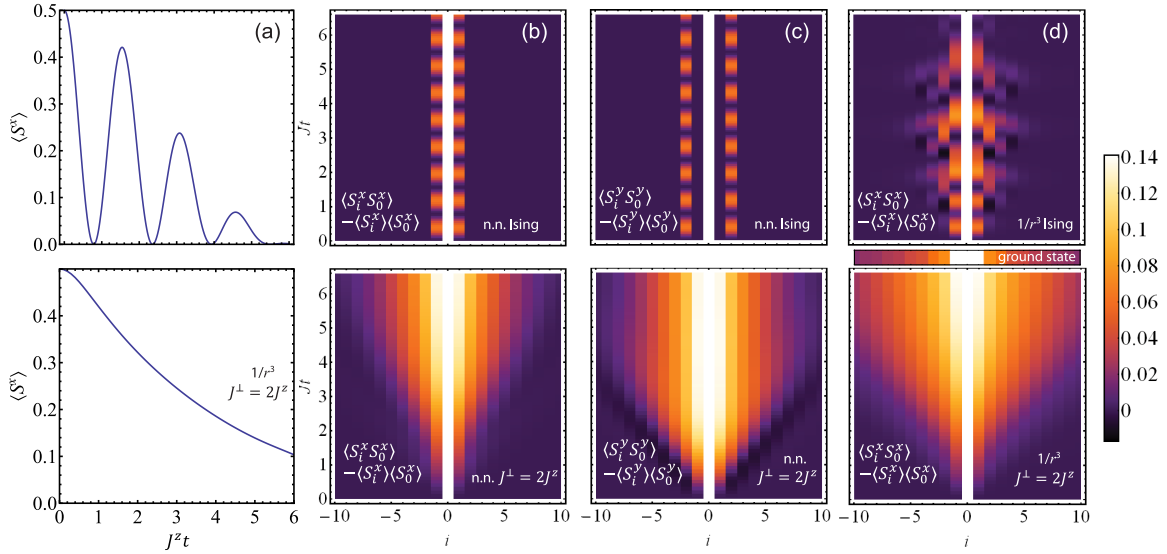
FIG. 4. (Color online) The dynamics of $\langle S^x(t) \rangle$ and correlation functions for the Ising and XXZ models in one dimension with positive (antiferromagnetic) couplings. Panel (a) shows $\langle S^x(t) \rangle$ versus t for $\varphi = \pi/2$ and $\alpha = 3$ for the Ising model (top) and XXZ model with $J_\perp = 2J_z$ (bottom). For $\varphi = \pi/2$, $\langle S^y \rangle = \langle S^z \rangle = 0$ due to symmetry considerations. The XXZ case is overdamped for this $J_\perp = 2J_z$ case (and, in general, for large $J_\perp > J_z$), while the Ising dynamics damps only when many different values of J_{ij} contribute to the dynamics. Other initial spin angles φ are similar, but while $\langle S^z \rangle \neq 0$ remains constant there is an additional precession or diffusion of the Bloch vector in the x-y plane. (b) Density plot of the two-point correlation function $\langle S_i^x S_j^x \rangle - \langle S_i^x \rangle \langle S_j^x \rangle$ versus $i - j$ (averaging over possible j's to reduce finite-size effects) and time for the nearest-neighbor Ising model (top) and XXZ model with $J_\perp = 2J_z$ (bottom). (c) Same as panel (b), but showing $\langle S_i^y S_j^y \rangle - \langle S_i^y \rangle \langle S_j^y \rangle$. (d) Same as panel (c), but for $\alpha = 3$ interactions rather than nearest neighbor. The ground-state correlations are shown above the dynamics for the $J^\perp = 2J^z$ case.

x-polarized, $\varphi = \pi/2$ initial state. The concurrence reaches its maximum value for $d/2 < \alpha < d$ and also persists for the longest time in this region. Similar to the entanglement entropy in Fig. 2(b), the effect of oscillations that emerge in the single- and two-spin correlation functions for $\alpha > d$ (here $d = 1$) can be seen for $\alpha \gtrsim 1.8$. Figure 2(f) shows the concurrence in the (φ, t) plane for $\alpha = 3/4$. Similar to other entanglement measures, the concurrence reaches its maximum value at $\varphi = \pi/2$. Away from this value, the growth of the concurrence is weaker and slower.

Summary of Sec. IV B. For each of the entanglement measures studied here, we find a qualitative crossover in behavior as the exponent α is varied. The concurrence reaches a local maximum in $\alpha \in (d/2, d)$, while the spin squeezing goes from evolving at a rate essentially independent of α for $\alpha > d$ to a rate increasing with α for $\alpha < d$. The choice of the entanglement measure also determines the time scales at which the maximum entanglement is reached. For all of the entanglement measures, an initial state in the x-y plane ($\varphi = \pi/2$) is optimal for the creation of maximum entanglement under time evolution.

V. ONE-DIMENSIONAL CORRELATIONS AND ENTANGLEMENT

In this section we investigate more general couplings with $J_{ij}^\perp \neq 0$, and we consider time scales much longer than the ones in which our perturbative short-time expressions of Sec. III are valid. To accomplish this we focus on one-dimensional systems with open boundary conditions, which are amenable to the adaptive t-DMRG [33–36]; we use a Krylov-space

implementation to treat the long-range interactions [117]. In addition to allowing us to investigate the $J_\perp \neq 0$ dynamics at relatively long times, the t-DMRG also allows us to compute entanglement entropies associated with arbitrary bipartitions of the system. We show that some features of the Ising limit, such as the types of correlations and the time scales on which they develop, are preserved in this model, while other features are modified, such as the range and propagation of the correlations. These results give insight into when one can extrapolate the behavior of the Ising solution to more general cases and help to elucidate the structure responsible for the solvability of the Ising limit.

Figure 4 compares and contrasts the dynamics of $\langle S^x(t) \rangle$ and some representative two-point correlation functions in the Ising limit and in the more general XXZ model with positive (antiferromagnetic) couplings. Figure 4(a) shows the time-evolution of $\langle S^x(t) \rangle$ for $J_\perp = 0$ (Ising, top) and $J_\perp = 2J_z$ XXZ (bottom) models with $1/r^3$ interactions, for an initial tipping angle of $\varphi = \pi/2$. (Similar results for $\langle S^x(t) \rangle$ were presented in Ref. [95].) The key difference between $\langle S^x(t) \rangle$'s evolution for the Ising and XXZ cases is that the former oscillates substantially, while the latter is overdamped (although we note that for $\alpha \lesssim d/2$ the Ising dynamics can become overdamped). The frequency spectrum of the dynamics provides a simple way to understand this behavior. In the Ising case, the frequency spectrum consists of all possible sums and differences of the coupling constants J_{ij}, as can be seen from Eq. (11). For $1/r^3$ (i.e., $\alpha = 3$) interactions in one-dimensional only a few frequencies are relevant over the time scale of interest, resulting in the pronounced oscillations. The same remains true for any interaction that decays sufficiently fast in

real space. In contrast, for the XXZ model, numerous other frequencies enter the spectrum (a continuous band of them emerges in the large-system limit), leading to an overdamped decay even for short-range interactions.

Figure 4(b) compares the Ising and XXZ dynamics of the spin correlation function $\mathcal{G}_{ij}^{xx}(t)$ for nearest-neighbor interactions as a function of the site separation $i - j$ and time (horizontal and vertical axes, respectively). We show the results for nearest-neighbor interactions because they highlight a crucial distinction between Ising and general XXZ dynamics. Whereas these correlations in the Ising case propagate only to a distance determined by the range of the interaction, for the XXZ case, they can propagate further. This propagation in the XXZ case is evident in the "light cone" [118–121] structure [122] in the bottom panels of Fig. 4(b). The restriction of the Ising limit correlations to a finite range can be seen from the results in Eq. (22) and has a simple physical explanation: In the Ising model, these correlations only build up due to direct interaction between two sites and not due to propagation of excitations through repeated interactions. This distinction between Ising and XXZ dynamics is expected to hold in higher dimensions as well, where the Ising correlations still fail to propagate while the XXZ correlation will continue to do so, although the XXZ propagation likely will not remain ballistic. Figure 4(c) shows the same phenomenon for $\mathcal{G}_{ij}^{yy}$; the only distinction is that the maximum distance between correlated sites in the Ising limit is twice as large as the range of the interaction.

In fact, this feature is quite general: All two-point correlations (namely, $\mathcal{G}^{ab}$ with $a, b \in \{x, y\}$) for interactions with range R are nonzero only within a radius of $2R$. The correlations can build up to twice the interaction range because a spin at site i can correlate two spins at sites $i + R$ and $i - R$ with each other, even though these two spins are a distance $2R$ apart. Sites that are further apart remain uncorrelated. We note that the extra structure for the $\mathcal{G}^{xx}$ and $\mathcal{G}^{yy}$ correlators in the top panels of Figs. 4(b) and 4(c)—namely, that $\mathcal{G}^{xx}$ correlations extend to only half that distance and that $\mathcal{G}^{yy}$ correlations occur only at a separation of 2 and not at shorter ranges—is a peculiarity of these specific correlation functions for nearest-neighbor interactions.

The correlations built up during the dynamics are, after very short times, larger than those in the ground state: Figure 4(d) shows the ground-state correlations above the bottom panel. Although we do not expect the ground-state correlations to be quantitatively similar to the transient dynamics we observe (nor to the steady state that this dynamics presumably approaches), this comparison provides a useful reference point to compare to the out-of-equilibrium correlations.

Turning from correlations to entanglement, we quantify two types of entanglement generated during the dynamics: spin squeezing ξ and the von Neumann entanglement entropy S_ℓ defined for a bipartitioning between sites ℓ and $\ell + 1$. Spin squeezing characterizes the temporal growth of metrologically useful entanglement, but since it is a spatially averaged quantity it yields no information about the spatial structure of the entanglement. On the other hand, the entanglement entropy S_ℓ reveals both the temporal and the spatial dependence of the entanglement and is closely related to the numerical
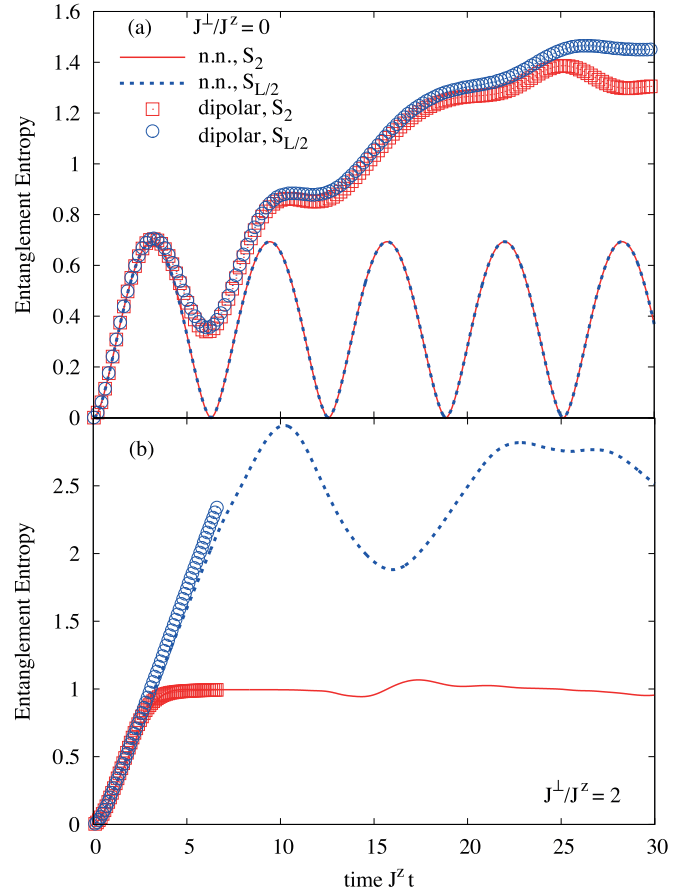

FIG. 5. (Color online) Adaptive t-DMRG results for the time evolution of the entanglement entropy for $N = 20$ site XXZ chains with nearest-neighbor interactions (lines) and dipolar interactions (symbols). (a) $J^\perp/J^z = 0$ (Ising); (b) $J^\perp/J^z = 2$ (XXZ). The plots display the entropy S_2 for a bipartition of size $\ell = 2$ at the edge of the systems (red) and $S_{L/2}$ at the center of the systems (blue). Note that in the Ising case the size of the bipartition does not play a role (nearest-neighbor case) or is of minor relevance (dipolar case) so that the results are identical, up to boundary effects coming into play in the dipolar case.

difficulty of simulating the dynamics with tensor-network-based algorithms.

The spin-squeezing dynamics for this model was calculated in Ref. [95], where it was found to grow and reach a maximum on a time scale on the order of $1/J^\perp$ or $1/J^z$ and then to shrink and disappear; Fig. 5 shows, in contrast, typical behavior for the time dependence of entanglement entropy. At the beginning of the time evolution, the entropy S_ℓ grows independently of ℓ. After a time that depends on the distance to the edge ℓ, the entropy stops growing. This happens first at the edges, then the time for this saturation increases with distance to the edge. This gives rise to an entropy that increases with ℓ, shown in Fig. 6. This should be contrasted to the ground states of both gapped and gapless systems: In gapped systems there will be no dependence on ℓ for distances larger than a correlation length, and in gapless systems there will be a logarithmic increase with distance to the edge [126,127]. As can be seen in Fig. 6, the entanglement in the nonequilibrium setup can be much larger than in equilibrium, even showing a linear dependence
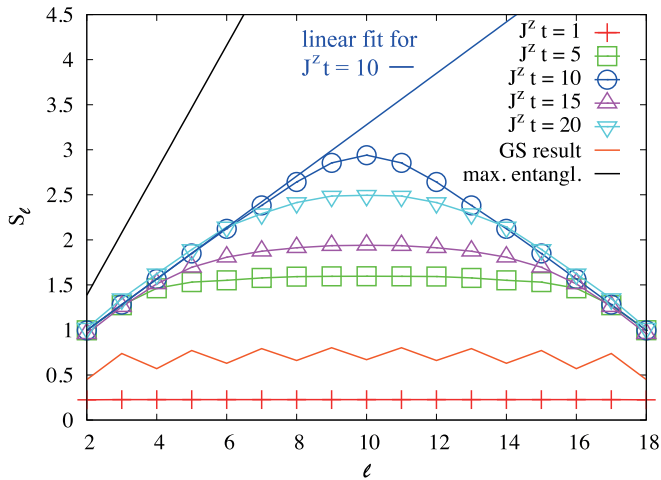
FIG. 6. (Color online) Adaptive t-DMRG results for the entanglement entropy of an $N = 20$ site XXZ chain with $J^\perp/J^z = 2$ and nearest-neighbor interactions as function of bipartition size at different instants of time. We compare to the ground-state result for the same system with open boundary conditions in the red curve ("GS result"). Note the linear increase at the flanks (a fit is shown by the solid blue line), which appears to reach a maximum slope in the course of the evolution. This is compared to the slope obtained for a maximally entangled state (labeled by "max. entangl.").

on the distance to the edge. At very long times, the entropy in the center of the chain can oscillate in time, possibly due to finite-size/boundary effects, as seen in Fig. 5 (these oscillations are similar to those found in Ref. [128], which indeed damp at long times for large system sizes).

The entanglement entropy in the Ising limit is quite different. Rather than increasing linearly with distance ℓ, the entanglement entropy is essentially independent of ℓ except near the edge. This is due to the lack of propagation of entanglement beyond a finite distance in short-ranged Ising models. The $1/r^3$ interaction in one dimension is sufficiently short-ranged that the main features of its dynamics can be understood from the behavior of the short-range dynamics. Thus, although there will be a weak dependence on ℓ, S_ℓ will be nearly zero for $\ell \gg \ell'$, where $\ell' = (Jt)^{1/3}$ grows rather slowly with time.

The strong quantum fluctuations away from the Ising and the Heisenberg limits can induce strong entanglement, and it is natural to ask how close we can come to the maximum possible value. We do this by considering the entanglement growth as a function of bipartition size at the edge of the system for sufficiently long times. As shown in Fig. 6, typically the entropy at the edge grows linearly, i.e.,

$$S_\ell = s\ell, \qquad (28)$$

where the slope s is the entanglement entropy density near the system edge. For spin-$\frac{1}{2}$ systems, a maximally entangled state is characterized by $S_\ell = \log(2^\ell) = \ell \log 2$ and thus $s = \log 2$. Hence, a maximally entangled state is characterized by a volume law rather than an area law [126,127]. Although our finding of a linearly increasing entropy indeed indicates a volume law at sufficiently long times, the value of s obtained is always substantially lower than the maximally entangled
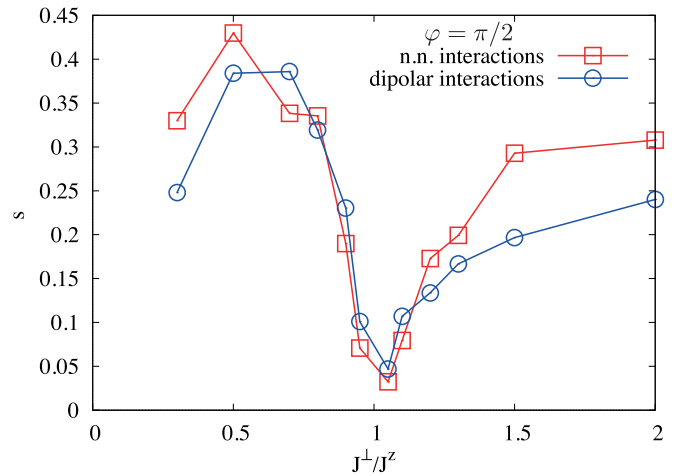

FIG. 7. (Color online) Maximal slope s of the entanglement entropy's dependence on the distance to the system edge, defined by $S_\ell = s\ell$ near the edges of the system, obtained during the time evolution as a function of $J^\perp/J^z$ for $\varphi = \pi/2$. Red line (squares), nearest-neighbor interactions; blue line (circles), dipolar interactions. Note that the slope (and hence the entanglement at the edges of the systems) appears to be larger for the nearest-neighbor interaction than for the dipolar interactions when $J^\perp > J^z$.

log 2. Figure 7 shows s as a function of $J^\perp/J^z$ for the quenches considered and for the cases where we could identify this volume law behavior [129]. As can be seen, a maximal value of $s \sim (2/3) \log 2$ is obtained for $J^\perp/J^z \sim 0.5$; it also increases to $\sim 1/3$ as $J^\perp/J^z \to \infty$, and it approaches zero at the Heisenberg point $J^\perp \approx J^z$. The behavior is similar for both nearest-neighbor and dipolar interactions. Note that, surprisingly, for $J_\perp > J_z$, s is actually larger for nearest-neighbor interactions than for long-range interactions.

VI. UNIVERSALITY OUT OF EQUILIBRIUM

In this section we demonstrate how the considered dynamic protocol can reveal nonequilibrium universality, dynamics having characteristic features that are insensitive to changes of the microscopic model. The existence of a universal behavior in nonequilibrium systems is especially interesting for two reasons. First, it is nonperturbative; any perturbation theory in the Hamiltonian or time will depend on the microscopic details of the perturbation. Second, while universality in equilibrium systems is explained by one of the most fundamental tools in physics, the renormalization group (RG), the required concepts and tools generalizing it to address many questions regarding far-from-equilibrium quantum systems have yet to be developed. (Though progress has been made in this direction, see, for example, Refs. [130–141]. Refs. [37–42] also provide useful examples of universal nonequilibrium behavior.)

The existence of universal behavior has been previously studied in related quenches, including quenches of quantum spin-$\frac{1}{2}$ chains. The main new insight provided here is not the existence of this behavior, but rather finding a quench procedure in which the universal behavior can be experimentally observed in a more feasible way than prior protocols proposed

for spin systems. The experimental feasibility is a consequence of two features of our quench protocol. First, the initial state we consider is trivial to prepare, in contrast to prior studies, which often required thermal equilibrium with temperatures much smaller than the spin-spin interactions, and thus hard to reach with current technology. Second, we need only to measure the global $\langle S^x \rangle$, a simple experimental task, while many previous proposals require measuring the long-distance asymptotic correlation functions, which is a much more difficult experimental task. Also, the results highlight a second sense of universality that emerges in these systems.

We consider the dynamics of an initial state with tipping angle $\varphi = \pi/2$, evolving under a one-dimensional XXZ Hamiltonian that deviates only slightly from the SU(2) symmetric point, i.e., $|J^\perp / J^z - 1| \ll 1$. However, although the explicit formulas will change, the existence of the universal singularity persists for arbitrary φ. Since the initial state is a ground state when $J^\perp = J^z < 0$, the dynamics can be understood as a small quench starting from the ground state at the SU(2) symmetric point, as in Fig. 1(b). We consider the case $J^\perp / J^z > 1$ so that the ground state of the XXZ Hamiltonian governing the time-evolution has gapless excitations. For the observable $\langle S^x(t) \rangle$, the overall sign of the Hamiltonian is irrelevant for the dynamics, although it is necessary that $J^\perp$ and J^z have the same sign. However, throughout this section we assume a ferromagnetic coupling $J^\perp < 0$, where the arguments are clearest. For simplicity, we restrict our attention in the exact numerics to nearest-neighbor interactions, $J_{ij}^{\{\perp,z\}} = J^{\{\perp,z\}}(\delta_{j,i+1} + \delta_{j,i-1})$.

Given that we are in the "small" quench regime, it is plausible that a low-energy description of the final Hamiltonian is appropriate to account for the dynamics. We first determine the low-energy theory near the SU(2) symmetric point, $J^\perp = J^z = -J$. We do this by writing the Hamiltonian as $H = H_0 + \delta H$ with H_0 the SU(2) symmetric point Hamiltonian and δH the deviation from it. At the SU(2) symmetric point the low-energy excitations are spin waves (delocalized single spin flips) that have a quadratic dispersion. By symmetry, the corresponding Hamiltonian is

$$H_0 = J \int dk\, k^2 \left(a \Pi_k^2 + b \phi_k^2\right), \tag{29}$$

where ϕ is the bosonized field [142], Π is its canonical conjugate, a and b are model-dependent constants whose values are unimportant here, and higher-order RG-irrelevant terms have been dropped. This form is expected since at the SU(2) Heisenberg point, the elementary excitations are noninteracting spin waves, behaving as free bosons with a k^2 dispersion. To utilize this low-energy theory, we need to relate physical observables to the field ϕ. For initial states in the x-y plane ($\varphi = \pi/2$), the field ϕ measures the in-plane direction of the (coarse-grained) local magnetization,

$$S^x = N/2 \cos(\phi), \tag{30}$$

where N is the number of spins and the field Π satisfies $S^z = \Pi/2$. We note that these definitions satisfy the commutation relation $[S^x, S^z] = (-i/2)S^y$ since $[N/2 \cos\phi, \Pi/2] = -(i/2)(N/2)\sin\phi$.

Adding a finite $\delta J \equiv J^z - J^\perp$ induces interactions between the freely dispersing bosons. In particular, the perturba-

tion to the Hamiltonian from the SU(2) point when $0 < \delta J \ll 1$ is $\delta J \sum_i S_i^z S_{i+1}^z$, which in the low-energy theory becomes

$$\delta H = \gamma \delta J \int dk\, |\Pi_k|^2, \tag{31}$$

where γ is an unimportant model-dependent proportionality constant, and we have again neglected RG-irrelevant terms. Therefore, the total Hamiltonian H to leading order in δJ, k is

$$H = \frac{v}{2} \int dk \left(\frac{2\pi}{K}|\Pi_k|^2 + \frac{K}{2\pi}k^2|\phi_k|^2\right), \tag{32}$$

the Luttinger liquid Hamiltonian with Luttinger parameter $K = 2\pi\sqrt{bJ/\gamma\delta J}$ and velocity $v = 2\sqrt{\gamma bJ\delta J}$, again neglecting RG-irrelevant terms. Both K and v have a singular $\sqrt{\delta J}$ dependence. (This equation can also be obtained by a Bogoliubov expansion for small δJ.) We return to the universality of these predictions later.

Now we compute the dynamics for the initial state evolving under Eq. (32), assuming this low-energy theory suffices for this computation. Using the relation Eq. (30) and the fact that Eq. (32) is Gaussian in ϕ, we have $\langle S^x(t) \rangle = N/2 \exp(-1/2\langle \phi^2 \rangle)$. Following Ref. [143], we find three qualitatively different types of behavior depending on the time,

$$\langle S^x(t) \rangle \propto \begin{cases} [1 - (\delta J t)^2] & \text{for } t \ll 1/\delta J, \\ e^{-t/\tau} & \text{for } 1/\delta J \ll t \ll N/v, \\ e^{-(t/\tau_{\text{fs}})^2} & \text{for } t \gg N/v. \end{cases} \tag{33}$$

Here $\tau = 4aK^2/(\pi^2 v)$, a is the lattice spacing, $\tau_{\text{fs}}^2 = \tau L/(2v)$, and L is the chain length (assumed to be large). The crucial observation is that near the SU(2) point these parameters follow a universal power law. In particular,

$$\tau = A\sqrt{J/\delta J^3} \tag{34}$$

(with some nonuniversal numerical prefactor A). This leads to a universal spin coherence decay time in the intermediate-time regime $1/\delta J \ll t \ll N/v \sim N/\sqrt{\delta J J}$ (thus, the appropriate separation of scales for this regime to exist is $N \gg \sqrt{J/\delta J}$). Physically, the spin dynamics in this regime results from dephasing of the initially populated Luttinger liquid excitations [144].

The intermediate-time result demonstrates the nonperturbative nature of the dynamics, since $e^{-t/\tau}$ with $\tau \propto \sqrt{J/\delta J^3}$ is nonanalytic in $J^z t$ and $J^\perp t$. Consequently, no order of perturbation theory in the bare Hamiltonian Eq. (1) would reproduce these results. This nonanalyticity requires the short-time expansion $[1 - (\delta J t)^2]$ and the intermediate-time expansion $(e^{-t/\tau})$ to have different functional forms and no time regime where they agree. We note that if $\langle S^x(t) \rangle$ is smooth, as it appears to be, this nonanalyticity is signaled as a divergence somewhere in the complex $J^z t$ or $J^\perp t$ plane. In this regard, our results resemble the dynamic singularities found on the real-time axis in Ref. [145].

The derivation of our intermediate-time dynamics also suggests that the results are universal, in two senses. The first sense of universality is that the dynamics depends only on the Luttinger parameter K and velocity v. Contrast this with the short-time behavior in Eqs. (4), which depends on the detailed couplings of the model. Irrelevant perturbations to the model (such as a second-nearest-neighbor coupling)

affect the short-time dynamics but not the intermediate-time dynamics, once written in terms of the Luttinger parameter. Physically, at these times, any high-energy degrees of freedom have had time to dephase and stop contributing to $\langle S^x(t)\rangle$ so that only the low-energy excitations governed by Luttinger liquid theory contribute. The second sense of universality is a further insensitivity to microscopic perturbations and is related to the fact that we are quenching from the SU(2) point. Here the Luttinger parameters and thus $\tau \propto K^2/v$ is a universal power law proportional to $\sqrt{J/\delta J^3}$.

Although the preceding analysis argued for universality based on Luttinger liquid theory, it does not determine the range of $J_\perp - J_z$ and system sizes N for which its conclusions are valid. To evaluate these parameter regimes, we use t-DMRG on chains with open boundary conditions, implemented with time-evolving block decimation (TEBD) in the ALPS package [146,147]. Figures 8(a) and 8(d) show the dynamics of $\langle S^x(t)\rangle$ for $\varphi = \pi/2$ and several quenches of chains with lengths up to $N = 90$ sites, differing in the final value of δJ. Exponential decay is evident at intermediate times when this regime is accessible to the numerics, in accord with the Luttinger liquid prediction in Eq. (33). (As an aside we note that for the specific model studied here, it may be possible to employ recently developed exact analytic methods [148] to study much of the time dynamics.)

Figure 8(e) shows the dependence of the exponential decay exponent τ on δJ. We determine τ by fitting the intermediate-time behavior of $\langle S^x(t)\rangle$ to an exponential decay for each δJ. Figures 8(a)–8(d) show these fits as dashed red lines. Specifically, we fit to times $0 < t < t_{\rm fit}$, where $t_{\rm fit}$ is defined by $\langle S^x(t_{\rm fit})\rangle = \langle S^x(0)\rangle/4$. In addition to long times, short times should also, in principle, be excluded from the fit, but for all of the $t_{\rm fit}$ presented here, the contribution from short times is negligible. We note therefore that the fit is accurate only over an intermediate window, which gets larger for smaller δJ and larger system sizes N. In this time window, $\langle S^x\rangle$ changes by about a factor of three, for our largest N and smallest δJ. Although confidently extracting a power law to high accuracy from such a narrow window is potentially problematic, we soon see that this window suffices to show consistency with the predicted power law with an error less than about 10%. Furthermore, it is important to investigate moderate system sizes and time scales, as these are comparable to the ones that may be currently accessible in cold-atom experiments.

Indeed, the results in Fig. 8(e) are consistent with the prediction of Eq. (34): that $\tau \propto \sqrt{J/\delta J^3}$ for small δJ. This is further quantified by Fig. 8(f), which shows the numerical derivative of the log-log plot in Fig. 8(e). By construction, this slope extracts the exponent of a power-law dependence of τ on δJ, and we find that it approaches $-3/2$ quite accurately for large systems and small δJ; even for large $\delta J \approx 0.3J$, the slope is around -1.6.

In order to reach this universal regime, one must go to times long compared to the microscopic cutoff time, which is $O(\delta J^{-1})$. However, in small systems, finite-size effects begin to play a role before reaching this universal regime. Thus, the characteristic scale is set by δJt, coinciding with the mean-field time scale $\tau \sim \delta J^{-1}$, which indeed appears to be approached for small systems, as shown in Fig. 8 (solid line).
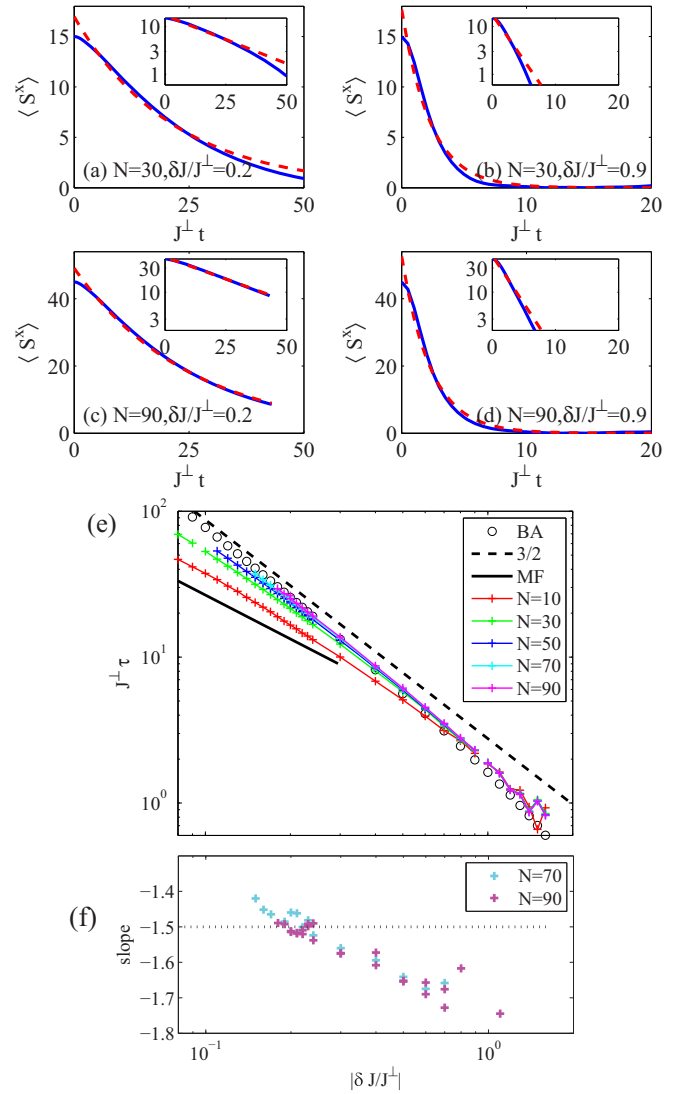

FIG. 8. (Color online) Universal scaling in far-from-equilibrium dynamics. (a)–(d) Dynamics of $\langle S^x(t)\rangle$ for two different values of the quench parameter $\delta J = J_\perp - J_z$ and of the system size L. Solid lines are t-DMRG results, and dashed lines are exponential fits $A_0 e^{-t/\tau}$ over the appropriate intermediate-time region (see main text). (e) Decay time τ as a function of the quench parameter δJ. Open circles, universal result, Eq. (34), with Luttinger liquid parameters determined by Bethe ansatz (BA); dashed line, universal scaling $J\tau \propto (J/\delta J)^{3/2}$, valid for $|\delta J/J_\perp| \ll 1$; joined symbols, t-DMRG results for various system sizes from $L = 10$ to $L = 90$. Large systems converge to the universal Luttinger liquid prediction, while small systems follow a mean-field (MF) behavior $\tau \propto \delta J^{-1}$. (f) The slope of the log-log plot in (e) for $N = 70$ and 90, obtained by numerical differentiation

Going beyond the limit of universal power-law scaling of τ (i.e., small δJ), we can compute the expected $\tau = 4K^2a/(\pi^2 v)$ by using Luttinger liquid parameters K and v that can be determined by the Bethe ansatz [149]. We see that even for some δJ large enough that the $\delta J^{-3/2}$ scaling breaks down, τ is still related to the Luttinger liquid K and v in the appropriate regime, confirming universality in the first sense described above.

We note that we have concentrated on $\{J_\perp, J_z\} < 0$, but for $J_z > 0$ (or equivalently $|\delta J/J^\perp| > 1$) the universal behavior breaks down even in this first sense: The numerical calculations show a significant deviation from the Luttinger liquid theory predictions. In this $J^z > 0$ regime, the initial state is far away from the actual ground state of the system. (For $J^z > |J^\perp|$, the ground state is qualitatively different, becoming antiferromagnetic rather than ferromagnetic.) As a consequence the dynamics is probably not well described by the Luttinger liquid theory. Further analytic and numerical calculations are needed in order to elucidate the long-time behavior in this regime and determine the possible emergence of a new universal behavior. Some calculations exploring this were presented in Ref. [150].

We conclude this section with an outlook based on our findings. Although we focused on one-dimensional systems, our results suggest that a universal behavior could be observed in higher-dimensional systems as well, where low-energy effective theories may continue to describe the dynamics after a small quench. However, even if this holds in higher dimensions, a suitable framework is still lacking for two reasons: (1) it is harder to identify the low-energy theories and (2) the dynamics of these low-energy theories is significantly harder to calculate; it is frequently intractable to present techniques. Ideas suitable for a more general quench that are based on real-time RG have been proposed and developed in Refs. [135–137,151,152], and for some quench scenarios conformal field theory [118], truncated Wigner approximation [134], and semiclassical approaches have been employed [141].

An interesting aspect of our results is that they provide a route to observing Luttinger liquid physics in ultracold lattice spin systems that does not require temperatures below the reach of ongoing cold-atom experiments (as opposed to more easily accessible Luttinger liquid physics associated with the density degree of freedom). In contrast to the current dynamic proposal, the observation of Luttinger liquid physics in spin systems in equilibrium requires cooling to (currently unfeasible) temperature scales much smaller than the magnetic interaction scale, which can be ∼1 nK for superexchange-based implementations in ultracold atoms [153]. This is true even for proposals that rely on nonequilibrium probes of equilibrium states, such as Ref. [154]. In our procedure, the initial state is easily prepared, and the dynamics is used to probe the Luttinger liquid physics. Observing the dynamics governed by the Luttinger liquid physics requires reaching time scales that are long compared to those determined by the magnetic interaction. However, even for a superexchange scale typical in cold-atom experiments (∼1 nK), the corresponding time scale is ∼50 ms and ought to be experimentally accessible.

VII. PHYSICAL REALIZATIONS

Specific instances of the XXZ Hamiltonian in Eq. (1) and the dynamical protocol discussed in this paper can be implemented in a variety of atomic, molecular, optical, and solid-state systems, including but not limited to polar molecules [8,9], trapped ions [17,18,63,64,155], Rydberg atom ensembles [12,156,157], magnetic quantum gases [69], neutral atoms in optical lattices [67,158], alkaline-earth-atom optical lattice clocks [22,24], tilted Bose-Hubbard models in optical lattices [159], magnetic defects in solids (e.g.,

nitrogen-vacancy centers in diamond) [160], and quantum magnetic materials in solid-state physics. For these solid-state systems, Refs. [28–31] give theoretical overviews, and Ref. [161] is just one example of recent experiments probing quench dynamics similar to that considered here. The models are also important for molecular aggregates [162–164] and energy transport in large organic and biomolecules [165–170]. Experiments in many of these systems have measured the same or closely related quench dynamics to that considered herein. The diversity and scope of these various implementations is enormous, but here we attempt to give a brief review of some of the most promising implementations, including their unique benefits and limitations. Table I of Sec. II summarizes the relevant properties (e.g., spin-coupling structure, energy scales, coherence times, etc.) of several of the systems described below.

A. Quantum magnetism in polar molecules

Polar molecules pinned in optical lattices have numerous desirable qualities for the realization of spin Hamiltonians. They have a variety of internal degrees of freedom—hyperfine, rotational, vibrational, and electronic—spanning many orders of magnitude in energy, all of which, in principle, can be used to encode a spin degree of freedom [49,50,55,56,171]. Moreover, since long-range dipole-dipole interactions do not require wave-function overlap, they persist in the deep-lattice limit (where tunneling is negligible) and are typically quite strong: $J/h \sim 10^2$ Hz at ∼500 nm lattice spacings for KRb, a relatively weakly interacting molecule; for LiCs the interactions can be a hundred times larger. When rotational levels encode the spin degree of freedom, an Ising term can be induced by permanently polarizing the molecules with modest electric fields, while spin-exchange terms ($\propto J_\perp$) of comparable strength can arise from resonant microwave photon exchange. The recent experiments reported in Refs. [8,9] have demonstrated the existence of $J_z = 0$ exchange dynamics in KRb molecules first prepared in the ro-vibrational ground state, pinned in a three-dimensional optical lattice, and excited using the quench protocol described in this paper. Those experiments have additionally demonstrated the capability to control the interaction strength by choosing different rotational levels to represent the spin degree of freedom. In the future, the addition of dc electric fields and microwave or Raman dressing is expected to enable the simulation of the more general XXZ spin models that we consider here, and more [56,58,172,173]. Current challenges in quantum simulation with polar molecules include the production of the molecules themselves (so far only KRb has been successfully produced in its rotational, vibrational, and hyperfine ground state at motional temperatures near quantum degeneracy), achieving sufficiently high phase-space density (i.e., approaching unit filling in a lattice) [174,175], and understanding any relevant decoherence mechanisms.

B. Quantum magnetism in trapped ions

In existing implementations of trapped-ion quantum simulators, the ions are laser cooled to form either one-dimensional (rf-Paul trap) [17] or two-dimensional (Penning trap) [18]

crystals. Many of the same properties that have made trapped ions a leading platform for quantum computation make them especially promising and versatile as simulators of models of quantum magnetism. First, they possess long-lived hyperfine states, which form the spin degree of freedom in all quantum simulations using trapped ions to date. While the spin degrees of freedom of two $\gtrsim \mu$m separated ions do not interact directly on experimentally relevant time scales, the spin of an individual ion can be coupled to its motion via a spin-dependent force. Experimentally, this is induced by off-resonant stimulated Raman transitions. By modulating this force at a frequency μ, virtual phonons which mediate relatively large ($J \lesssim 10$ kHz) spin-spin couplings are excited. These spin-spin couplings inherit the nonlocal structure of the phonon modes, and hence are generically long-ranged; depending on how far μ is detuned from the various phonon modes of the ion crystal, the coupling between two ions falls off in space as an approximate power law of the distance between them, with exponent $0 \leqslant \alpha \leqslant 3$. To date, experiments have successfully implemented Ising ($J_\perp = 0$) [17,18,63] and XX ($J_z = 0$) [64,115] models both in and out of equilibrium, but, in principle, these systems can be used to realize generic anisotropic spin models ($J_x \neq J_y \neq J_z$) [65]. Current challenges in trapped ion quantum simulation are mainly related to scalability; pushing to larger system sizes adversely affects the ratio of the spin-spin interaction time scales to the system lifetime and may eventually require working in cryogenic environments. We note that there are a variety of possible complications due to the production of real phonon excitation during nonequilibrium dynamics in these systems [176]; the importance of these effects is only partially understood.

C. Quantum magnetism in Rydberg atoms

Very similar to polar molecules, Rydberg atoms possess a strong dipole-dipole interaction. As the dipole moment is limited only by the size of the Rydberg atoms, their mutual interaction can be many orders of magnitude stronger than all other interactions between neutral atoms or molecules. If a pair of two excitations in Rydberg atoms is resonant with dipole-allowed transitions to other two-excitation states, then the dipolar coupling between them results in an anisotropic long-range $1/r^3$ interaction. If this so-called Förster process is off resonant, this gives rise to the well-known attractive or repulsive $1/r^6$ van der Waals interaction. The Förster resonance can be tuned and experimentally controlled in fast pulse sequences by electric fields that act differently on the involved Rydberg states, thus enabling one to control the detuning between the two-excitation states. Another experimental tool is microwave pulses, which can be used to induce oscillating dipole moments. This is an ideal tool in Ramsey-like pulse sequences. It is important to note that the lifetime of Rydberg atoms is limited typically to ~ 10 μs. However, coherent driving, as well as interaction time scales, have been shown to reach even the GHz level [177,178], which is ultimately limited only by the Kepler frequency, i.e., the energy splitting between adjacent Rydberg states. On these time scales it is not even necessarily required to work with a degenerate ultracold gas, as even at elevated temperatures the system behaves as a frozen gas on the microsecond time scale.

Strongly interacting frozen Rydberg gases have been shown to be able to quantum simulate the ground states of spin Hamiltonians. Following the theoretical prediction of a quantum phase transition from a paramagnetic to crystalline phase [66], the universal scaling behavior in the quantum critical regime was experimentally investigated and compared to *ab initio* and mean-field calculations [179]. Spatially ordered ground states have been observed by various methods [10,11], including in Ref. [12], which employed an underlying optical lattice. Ramsey sequences have been used to monitor the nonequilibrium dynamics and interaction [13–15]. Quenches to Förster resonant interaction were investigated as early as 1998 [180,181], and they have recently been used to investigate spatial diffusion processes [182].

D. Quantum magnetism of neutral atoms in optical lattices via dipolar interactions

Strong magnetic interactions between atoms with unpaired electrons give rise to mechanical effects in a trapped quantum gas that were observed in Ref. [183]. They also result in strong dipolar relaxation processes [68], which have been used for demagnetization cooling [184]. Reference [68] noted that the dipolar interaction can lead to an exchange term, but in free space this is always accompanied by a magnetization relaxation term. It was then demonstrated that in a dipolar lattice gas the relaxation of the magnetization can be suppressed [21], in which case the remaining terms of the dipolar interaction are of the form Eq. (1) with $J^\perp/J^z$ fixed by the nature of the dipolar interaction. Recently, an experiment in the many-body limit with singly and doubly occupied lattices sites was performed and showed evidence for coherent intersite spin exchange dynamics [69]. So far these experiments have been performed with chromium atoms, which have a magnetic moment of 6 μ_B, where μ_B is the Bohr magneton, and a ground-state manifold with a spin $S = 3$ degree of freedom. Upcoming experiments with erbium (7 μ_B) and dysprosium (10 μ_B) promise even stronger couplings [19,20].

E. Quantum magnetism of neutral atoms in optical lattices via superexchange

Neutral atoms in optical lattices furnish natural realizations of Bose- or Fermi-Hubbard models [185]. Much like the electrons in real materials, at unit filling and in the strongly interacting limit these atoms form Mott insulators with one particle per lattice site [186–188]. If each atom can be in one of two hyperfine (spin) states, virtual excitations into states away from unit filling, i.e., with holes and double occupancies, mediate spin-spin interactions between neighboring atoms that are ferromagnetic (antiferromagnetic) for bosons (fermions). By choosing internal states that have different scattering properties, or by using hyperfine-state-dependent lattices, or both, it is possible to tune the relative strength of J_z and $J_\perp$ [189]. These superexchange interactions have been probed in bosonic Rb atoms via nonequilibrium dynamics in double-well arrays [67] and recently in equilibrium in anisotropic lattice geometries using low-temperature fermionic Mott insulators [158]. However, due to the very small superexchange energy scales ($J \lesssim 100$ Hz, often much

less), studying equilibrium properties of fermionic systems in the temperature regime where long-range antiferromagnetic order exists remains elusive. In alkaline-earth atoms, the independence of the scattering properties on the nuclear spin I allows for superexchange models with SU($N = 2I + 1$) [rather than SU(2)] symmetry [190–193]. Recently, direct and indirect signatures of SU(N) symmetry in s- and p-wave collisions have been reported in Refs. [194–197]. Signatures of a superexchange processes respecting this enhanced SU(N) symmetry have not been demonstrated experimentally; however, the required low-entropy SU(N) Mott insulators with $N = 6$ have been recently created [195,197,198].

F. Quantum magnetism of alkaline-earth atoms in optical lattice clocks

Alkaline-earth atoms trapped in one- and two-dimensional optical lattices can realize spin models in appropriate limits. Here the role of lattice sites is played by single-particle quantized motional eigenstates (e.g., harmonic oscillator levels along the "tubes" or "pancakes" of this lattice), and the spin degrees of freedom are encoded in two electronic states (clock states) [25,84,196]. The spin-spin couplings arise from the direct overlap of single-particle wave functions, and because these systems must be dilute to avoid rapid two-body losses [199,200] typical spin-spin interaction energies are fairly small. However, the long-lived nature of the optically excited state, together with excellent coherence properties of state-of-the-art clock lasers [70,71,201], both make coherent spin-dynamics accessible in these systems [22–25]. If p-wave interactions are ignored, the spin-spin Hamiltonian is SU(2) symmetric ($J_z = J_\perp$), and no dynamics results from the collective initial states considered in this paper (inhomogeneous states do, however, have nontrivial dynamics [83–85,202]). The p-wave interactions induce an anisotropy $\tilde{J} = J_z - J_\perp$, which, while small, can still induce nontrivial dynamics (i.e., dynamics not described by short-time perturbation theory) for the collective initial states considered here, during time scales longer than hundreds of ms.

G. Quantum magnetism in tilted lattices

The method, proposed in Ref. [203] and realized in Refs. [159,204], leaves behind the typical approach of hyperfine-encoded spin states with superexchange mediated interactions. The key idea is that the low-energy manifold of a unit-filled Mott insulator, in the presence of a linear potential gradient, can be mapped onto the low-energy sector of a nearest-neighbor antiferromagnetic Ising model ($J_\perp = 0$, $J_z > 0$) in a transverse field. The smallest energy scale of the spin model is ultimately constrained by the tunneling energy in the lattice, which is about an order of magnitude larger than the superexchange scale that usually governs quantum magnetism of neutral atoms in optical lattices. The nonequilibrium dynamics described in this paper is only valid in the low tipping angle limit, because the mapping from a Bose-Hubbard model to the antiferromagnetic Ising model is only valid within the low-energy sectors of *both* models. This does not necessarily mean, however, that the universal aspects of the dynamics we considered cannot be explored

for weak quenches, where the dynamics is indeed governed by Eq. (8) plus an additional transverse field. Numerical simulations of the time evolution [205] that compare the quench dynamics starting from a pure spin-polarized state in the full Bose-Hubbard model and the spin model show agreement for various oscillations, thus confirming the validity of this observation.

VIII. CONCLUSIONS AND OUTLOOK

In this paper we have studied the dynamics of spin systems governed by a general XXZ Hamiltonian Eq. (1). In particular, we studied the time-evolution of an initially spin-polarized state, a protocol that can be viewed and experimentally implemented either as a quantum quench or as Ramsey spectroscopy. We found that the range and magnitude of correlations and entanglement out of equilibrium could become comparable to or larger than those exhibited by strongly correlated equilibrium ground states. In particular, in one dimension, we found that entanglement grows to satisfy a "volume law" over time. The steady state nevertheless is not maximally entangled. We also demonstrated an experimentally realistic procedure for which universal singular dynamics can manifest out of equilibrium.

To derive these results, we employed a variety of exact analytic and numerical methods. Necessarily, the exact methods were restricted to special cases: short times, the Ising limit ($J_{ij}^\perp = 0$), and one-dimensional systems. Alternative methods—even approximate ones—to study the more general cases are highly desirable. Among those one can mention: mean-field theories, the truncated Wigner approximation [206], cluster expansions [9,207–209], and linear response theory [210]. We expect that the exact results developed here will provide a foundation and test bed for those approximate methods.

Many additional intriguing aspects of the physics are opened up by slight modifications of the dynamical procedure, several of which may be experimentally implementable. For example, one could change the sudden quenches to quenches with a finite, variable rate and thereby explore Kibble-Zurek-type physics [211,212]. One could also work with inhomogeneous initial spin states, opening the possibility to study transport and other intriguing phenomena such as many-body localization [213–217], especially in systems with inhomogeneous and long-range couplings $J_{ij}^{\{\perp,z\}}$.

[1] A. Lamacraft and J. Moore, *Ultracold Bosonic and Fermionic Gases* (Elsevier, Oxford, UK, 2012), Vol. 5.

[2] N. Gedik, D.-S. Yang, G. Logvenov, I. Bozovic, and A. H. Zewail, Science **316**, 425 (2007).

[3] M. Kitagawa and M. Ueda, Phys. Rev. A **47**, 5138 (1993).

[4] J. J. Bollinger, W. M. Itano, D. J. Wineland, and D. J. Heinzen, Phys. Rev. A **54**, R4649 (1996).

[5] R. Raussendorf and H. J. Briegel, Phys. Rev. Lett. **86**, 5188 (2001).

[6] M. A. Cazalilla and M. Rigol, New J. Phys. **12**, 055006 (2010).

[7] A. Polkovnikov, K. Sengupta, A. Silva, and M. Vengalattore, Rev. Mod. Phys. **83**, 863 (2011).

[8] B. Yan, S. A. Moses, B. Gadway, J. P. Covey, K. R. A. Hazzard, A. M. Rey, D. S. Jin, and J. Ye, Nature (London) **501**, 521 (2013).

[9] K. R. A. Hazzard, B. Gadway, M. Foss-Feig, B. Yan, S. A. Moses, J. P. Covey, N. Y. Yao, M. D. Lukin, J. Ye, D. S. Jin, and A. M. Rey, Phys. Rev. Lett. **113**, 195302 (2014).

[10] A. Schwarzkopf, R. E. Sapiro, and G. Raithel, Phys. Rev. Lett. **107**, 103001 (2011).

[11] A. Schwarzkopf, D. A. Anderson, N. Thaicharoen, and G. Raithel, Phys. Rev. A **88**, 061406 (2013).

[12] P. Schauß, M. Cheneau, M. Endres, T. Fukuhara, S. Hild, A. Omran, T. Pohl, C. Gross, S. Kuhr, and I. Bloch, Nature (London) **491**, 87 (2012).

[13] W. R. Anderson, M. P. Robinson, J. D. D. Martin, and T. F. Gallagher, Phys. Rev. A **65**, 063404 (2002).

[14] B. Butscher, J. Nipper, J. B. Balewski, L. Kukota, V. Bendkowsky, R. Löw, and T. Pfau, Nat. Phys. **6**, 970 (2010).

[15] J. Nipper, J. B. Balewski, A. T. Krupp, B. Butscher, R. Löw, and T. Pfau, Phys. Rev. Lett. **108**, 113001 (2012).

[16] T. Lahaye, C. Menotti, L. Santos, M. Lewenstein, and T. Pfau, Rep. Prog. Phys. **72**, 126401 (2009).

[17] K. Kim, M.-S. Chang, S. Korenblit, R. Islam, E. Edwards, J. Freericks, G.-D. Lin, L.-M. Duan, and C. Monroe, Nature (London) **465**, 590 (2010).

[18] J. W. Britton, B. C. Sawyer, A. C. Keith, C.-C. J. Wang, J. K. Freericks, H. Uys, M. J. Biercuk, and J. J. Bollinger, Nature (London) **484**, 489 (2012).

[19] M. Lu, N. Q. Burdick, S. H. Youn, and B. L. Lev, Phys. Rev. Lett. **107**, 190401 (2011).

[20] K. Aikawa, A. Frisch, M. Mark, S. Baier, A. Rietzler, R. Grimm, and F. Ferlaino, Phys. Rev. Lett. **108**, 210401 (2012).

[21] A. de Paz, A. Chotia, E. Maréchal, P. Pedri, L. Vernac, O. Gorceix, and B. Laburthe-Tolra, Phys. Rev. A **87**, 051609 (2013).

[22] M. D. Swallows, M. Bishof, Y. Lin, S. Blatt, M. J. Martin, A. M. Rey, and J. Ye, Science **331**, 1043 (2011).

[23] N. D. Lemke, J. von Stecher, J. A. Sherman, A. M. Rey, C. W. Oates, and A. D. Ludlow, Phys. Rev. Lett. **107**, 103902 (2011).

[24] M. J. Martin, M. Bishof, M. D. Swallows, X. Zhang, C. Benko, J. von Stecher, A. V. Gorshkov, A. M. Rey, and J. Ye, Science **341**, 632 (2013).

[25] A. Rey, A. Gorshkov, C. Kraus, M. Martin, M. Bishof, M. Swallows, X. Zhang, C. Benko, J. Ye, N. Lemke, and A. Ludlow, Ann. Phys. **340**, 311 (2014).

[26] M. W. Doherty, N. B. Manson, P. Delaney, F. Jelezko, J. Wrachtrup, and L. C. Hollenberg, Phys. Rep. **528**, 1 (2013).

[27] J. R. Weber, W. F. Koehl, J. B. Varley, A. Janotti, B. B. Buckley, C. G. Van de Walle, and D. D. Awschalom, Proc. Natl. Acad. Sci. USA **107**, 8513 (2010).

[28] A. Auerbach, *Interacting Electrons and Quantum Magnetism* (Springer-Verlag, New York, 1994).

[29] S. Sachdev, Nat. Phys. **4**, 173 (2008).

[30] C. Lacroix, P. Mendels, and F. Mila (eds.), *Introduction to Frustrated Magnetism* (Springer, Heidelberg, 2011).

[31] S. Sachdev, *Quantum Phase Transitions*, 2nd ed. (Cambridge University Press, Cambridge, UK, 2011).

[32] The "numerically exact" method employed is the time-dependent density matrix renormalization group (t-DMRG) method [33–36]. What we mean by the term numerically exact is that there is a parameter that can, in principle, be increased until the method becomes arbitrarily accurate, and, moreover, that the errors can be quantified by techniques for scaling in this convergence parameter. Errors are typically expected to be smaller than or comparable to the point size in our plots.

[33] S. R. White, Phys. Rev. Lett. **69**, 2863 (1992).

[34] G. Vidal, Phys. Rev. Lett. **93**, 040502 (2004).

[35] A. J. Daley, C. Kollath, U. Schollwöck, and G. Vidal, J. Stat. Mech. (2004) P04005.

[36] S. R. White and A. E. Feiguin, Phys. Rev. Lett. **93**, 076401 (2004).

[37] A. J. Bray, Adv. Phys. **43**, 357 (1994).

[38] P. Calabrese and A. Gambassi, J. Phys. A: Math. Gen. **38**, R133 (2005).

[39] M. Henkel, H. Hinrichsen, and S. Lübeck, *Non-equilibrium Phase Transitions* (Springer, Netherlands, 2009), Vol. 1.

[40] M. Henkel and M. Pleimling, *Non-equilibrium Phase Transitions* (Springer, Netherlands, 2010), Vol. 2.

[41] A. Kamenev, *Field Theory of Non-equilibrium Systems* (Cambridge University Press, Cambridge, UK, 2011).

[42] U. C. Täuber, *Critical Dynamics: A Field Theory Approach to Equilibrium and Non-equilibrium Scaling Behavior* (Cambridge University Press, Cambridge, UK, 2014).

[43] K. I. Kugel and D. I. Khomskii, Sov. Phys. JETP **37**, 725 (1973).

[44] K. I. Kugel and D. I. Khomskii, Sov. Phys. Usp. **25**, 231 (1982).

[45] Z. Nussinov and J. van den Brink, arXiv:1303.5922.

[46] A. Kitaev, Ann. Phys. **321**, 2 (2006).

[47] H. Yao and S. A. Kivelson, Phys. Rev. Lett. **99**, 247203 (2007).

[48] Z.-X. Liu, Z.-B. Yang, Y.-J. Han, W. Yi, and X.-G. Wen, Phys. Rev. B **86**, 195122 (2012).

[49] R. Barnett, D. Petrov, M. Lukin, and E. Demler, Phys. Rev. Lett. **96**, 190401 (2006).

[50] M. L. Wall and L. D. Carr, Phys. Rev. A **82**, 013611 (2010).

[51] M. L. Wall and L. D. Carr, New J. Phys. **11**, 055027 (2009).

[52] J. Schachenmayer, I. Lesanovsky, A. Micheli, and A. J. Daley, New J. Phys. **12**, 103044 (2010).

[53] J. Pérez-Ríos, F. Herrera, and R. V. Krems, New J. Phys. **12**, 103007 (2010).

[54] F. Herrera, M. Litinskaya, and R. V. Krems, Phys. Rev. A **82**, 033428 (2010).

[55] A. V. Gorshkov, S. R. Manmana, G. Chen, E. Demler, M. D. Lukin, and A. M. Rey, Phys. Rev. A **84**, 033619 (2011).

[56] A. V. Gorshkov, S. R. Manmana, G. Chen, J. Ye, E. Demler, M. D. Lukin, and A. M. Rey, Phys. Rev. Lett. **107**, 115301 (2011).

[57] S. R. Manmana, E. M. Stoudenmire, K. R. A. Hazzard, A. M. Rey, and A. V. Gorshkov, Phys. Rev. B **87**, 081106 (2013).

[58] A. V. Gorshkov, K. R. A. Hazzard, and A. M. Rey, Mol. Phys. **111**, 1908 (2013).

[59] L. D. Carr, D. DeMille, R. V. Krems, and J. Ye, New J. Phys. **11**, 055049 (2009).

[60] D. Porras, J. I. Cirac, S. Kilina, S. Tretiak, and E. Einarsson, Phys. Rev. Lett. **96**, 250501 (2006).

[61] K. Kim, M.-S. Chang, R. Islam, S. Korenblit, L.-M. Duan, and C. Monroe, Phys. Rev. Lett. **103**, 120502 (2009).

[62] J. T. Barreiro, M. Müller, P. Schindler, D. Nigg, T. Monz, M. Chwalla, M. Hennrich, C. F. Roos, P. Zoller, and R. Blatt, Nature (London) **470**, 486 (2011).

[63] R. Islam, C. Senko, W. C. Campbell, S. Korenblit, J. Smith, A. Lee, E. E. Edwards, C.-C. J. Wang, J. K. Freericks, and C. Monroe, Science **340**, 583 (2013).

[64] P. Richerme, Z.-X. Gong, A. Lee, C. Senko, J. Smith, M. Foss-Feig, S. Michalakis, A. V. Gorshkov, and C. Monroe, Nature (London) **511**, 198 (2014).

[65] D. Porras and J. I. Cirac, Phys. Rev. Lett. **92**, 207901 (2004).

[66] H. Weimer, R. Löw, T. Pfau, and H. P. Büchler, Phys. Rev. Lett. **101**, 250601 (2008).

[67] S. Trotzky, P. Cheinet, S. Fölling, M. Feld, U. Schnorrberger, A. M. Rey, A. Polkovnikov, E. A. Demler, M. D. Lukin, and I. Bloch, Science **319**, 295 (2008).

[68] S. Hensler, J. Werner, A. Griesmaier, P. Schmidt, A. Görlitz, T. Pfau, S. Giovanazzi, and K. Rzazewski, Appl. Phys. B **77**, 765 (2003).

[69] A. de Paz, A. Sharma, A. Chotia, E. Maréchal, J. H. Huckans, P. Pedri, L. Santos, O. Gorceix, L. Vernac, and B. Laburthe-Tolra, Phys. Rev. Lett. **111**, 185305 (2013).

[70] N. Hinkley, J. A. Sherman, N. B. Phillips, M. Schioppo, N. D. Lemke, K. Beloy, M. Pizzocaro, C. W. Oates, and A. D. Ludlow, Science **341**, 1215 (2013).

[71] B. J. Bloom, T. L. Nicholson, J. R. Williams, S. L. Campbell, M. Bishof, X. Zhang, W. Zhang, S. L. Bromley, and J. Ye, Nature (London) **506**, 71 (2014).

[72] H. J. Lewandowski, D. M. Harber, D. L. Whitaker, and E. A. Cornell, Phys. Rev. Lett. **88**, 070403 (2002).

[73] J. M. McGuirk, D. M. Harber, H. J. Lewandowski, and E. A. Cornell, Phys. Rev. Lett. **91**, 150402 (2003).

[74] A. Kuklov, N. Prokof'ev, and B. Svistunov, Phys. Rev. A **69**, 025601 (2004).

[75] X. Du, L. Luo, B. Clancy, and J. E. Thomas, Phys. Rev. Lett. **101**, 150401 (2008).

[76] S. S. Natu and E. J. Mueller, Phys. Rev. A **79**, 051601 (2009).

[77] F. Piéchon, J. N. Fuchs, and F. Laloë, Phys. Rev. Lett. **102**, 215301 (2009).

[78] B. Mischuck, I. H. Deutsch, and P. S. Jessen, Phys. Rev. A **81**, 023403 (2010).

[79] W. Maineult, C. Deutsch, K. Gibble, J. Reichel, and P. Rosenbusch, Phys. Rev. Lett. **109**, 020407 (2012).

[80] H. K. Pechkis, J. P. Wrubel, A. Schwettmann, P. F. Griffin, R. Barnett, E. Tiesinga, and P. D. Lett, Phys. Rev. Lett. **111**, 025301 (2013).

[81] M. Koschorreck, D. Pertot, E. Vogt, and M. Köhl, Nat. Phys. **9**, 405 (2013).

[82] A. Widera, S. Trotzky, P. Cheinet, S. Fölling, F. Gerbier, I. Bloch, V. Gritsev, M. D. Lukin, and E. Demler, Phys. Rev. Lett. **100**, 140401 (2008).

[83] K. Gibble, Phys. Rev. Lett. **103**, 113202 (2009).

[84] A. M. Rey, A. V. Gorshkov, and C. Rubbo, Phys. Rev. Lett. **103**, 260402 (2009).

[85] Z. Yu and C. J. Pethick, Phys. Rev. Lett. **104**, 010801 (2010).

[86] E. L. Hazlett, L.-C. Ha, and C. Chin, arXiv:1306.4018.

[87] M. Knap, A. Kantian, T. Giamarchi, I. Bloch, M. D. Lukin, and E. Demler, Phys. Rev. Lett. **111**, 147205 (2013).

[88] T. Kitagawa, S. Pielawa, A. Imambekov, J. Schmiedmayer, V. Gritsev, and E. Demler, Phys. Rev. Lett. **104**, 255302 (2010).

[89] D. A. Abanin, T. Kitagawa, I. Bloch, and E. Demler, Phys. Rev. Lett. **110**, 165304 (2013).

[90] M. Atala, M. Aidelsburger, J. T. Barreiro, D. Abanin, T. Kitagawa, E. Demler, and I. Bloch, Nat. Phys. **9**, 795 (2013).

[91] M. Foss-Feig, K. R. A. Hazzard, J. J. Bollinger, and A. M. Rey, Phys. Rev. A **87**, 042101 (2013).

[92] M. Foss-Feig, K. R. A. Hazzard, J. J. Bollinger, A. M. Rey, and C. W. Clark, New J. Phys. **15**, 113008 (2013).

[93] M. van den Worm, B. C. Sawyer, J. J. Bollinger, and M. Kastner, New J. Phys. **15**, 083007 (2013).

[94] The state includes no fluctuations from this; formally, this is easiest to see by considering the state $|\Psi(0)\rangle \equiv \langle \cdots \downarrow\downarrow \cdots \rangle$ [note that since the Hamiltonian for $J_{ij}^z = J_{ij}^\perp$ is SU(2) symmetric for spin rotations, all rotations of this state are degenerate]. When H acts on this state, the flip-flop terms vanish, and the action of the Ising term is a c number times the state; this confirms that $|\Psi(0)\rangle$ is an eigenstate. Using $\langle \mathbf{S}_i \cdot \mathbf{S}_j \rangle \leqslant 1/4$, it can be shown that it saturates the minimum possible energy for the Hamiltonian (ground state) if $J_{ij}^\perp < 0$.

[95] K. R. A. Hazzard, S. R. Manmana, M. Foss-Feig, and A. M. Rey, Phys. Rev. Lett. **110**, 075301 (2013).

[96] D. M. Greenberger, M. A. Horne, and A. Zeilinger, in *Bell's Theorem, Quantum Theory, and Conceptions of the Universe*, edited by M. Kafatos (Kluwer, Dordrecht, 1989).

[97] G. G. Emch, J. Math. Phys. **7**, 1198 (1966).

[98] C. Radin, J. Math. Phys. **11**, 2945 (1970).

[99] M. Kastner, Phys. Rev. Lett. **106**, 130601 (2011).

[100] M. Kastner, Cent. Eur. J. Phys. **10**, 637 (2012).

[101] R. Horodecki, P. Horodecki, M. Horodecki, and K. Horodecki, Rev. Mod. Phys. **81**, 865 (2009).

[102] J. I. Cirac, *Entanglement in Many-body Quantum Systems*, Proceedings of the Les Houches Summer School of Theoretical Physics, 2010 (Oxford University Press, Oxford, 2012).

[103] K. Mølmer and A. Sørensen, Phys. Rev. Lett. **82**, 1835 (1999).

[104] J. Schachenmayer, B. P. Lanyon, C. F. Roos, and A. J. Daley, Phys. Rev. X **3**, 031015 (2013).

[105] D. J. Wineland, J. J. Bollinger, W. M. Itano, F. L. Moore, and D. J. Heinzen, Phys. Rev. A **46**, R6797 (1992).

[106] J. Ma, X. Wang, C. P. Sun, and F. Nori, Phys. Rep. **509**, 89 (2011).

[107] A. S. Sørensen and K. Mølmer, Phys. Rev. Lett. **86**, 4431 (2001).

[108] G. Tóth, C. Knapp, O. Gühne, and H. J. Briegel, Phys. Rev. Lett. **99**, 250405 (2007).

[109] G. Tóth, C. Knapp, O. Gühne, and H. J. Briegel, Phys. Rev. A **79**, 042334 (2009).

[110] A. Sorensen, L. M. Duan, J. I. Cirac, and P. Zoller, Nature (London) **409**, 63 (2001).

[111] J. K. Korbicz, J. I. Cirac, and M. Lewenstein, Phys. Rev. Lett. **95**, 120502 (2005).

[112] C. Gross, T. Zibold, E. Nicklas, J. Estève, and M. K. Oberthaler, Nature (London) **464**, 1165 (2010).

[113] J. Estève, C. Gross, A. Weller, S. Giovanazzi, and M. K. Oberthaler, Nature (London) **455**, 1216 (2008).

[114] W. K. Wootters, Phys. Rev. Lett. **80**, 2245 (1998).

[115] P. Jurcevic, B. P. Lanyon, P. Hauke, C. Hempel, P. Zoller, R. Blatt, and C. F. Roos, Nature (London) **511**, 202 (2014).

[116] The corresponding resource is the correlations that cannot be generated through quantum operations within each region and classical communication between them.

[117] S. R. Manmana, A. Muramatsu, and R. M. Noack, AIP Conf. Proc. **789**, 269 (2005).

[118] P. Calabrese and J. Cardy, Phys. Rev. Lett. **96**, 136801 (2006).

[119] A. M. Läuchli and C. Kollath, J. Stat. Mech.: Theory Exp. (2008) P05018.

[120] S. R. Manmana, S. Wessel, R. M. Noack, and A. Muramatsu, Phys. Rev. B **79**, 155104 (2009).

[121] M. Cheneau, P. Barmettler, D. Poletti, M. Endres, P. Schauß, T. Fukuhara, C. Gross, I. Bloch, C. Kollath, and S. Kuhr, Nature (London) **481**, 484 (2012).

[122] The strict light cone [123] must be generalized in the presence of interactions that are not finite ranged [64,115,124,125].

[123] E. H. Lieb and D. W. Robinson, Commun. Math. Phys. **28**, 251 (1972).

[124] M. B. Hastings and T. Koma, Commun. Math. Phys. **265**, 781 (2006).

[125] J. Eisert, M. van den Worm, S. R. Manmana, and M. Kastner, Phys. Rev. Lett. **111**, 260401 (2013).

[126] P. Calabrese and J. Cardy, J. Stat. Mech.: Theory Exp. (2004) P06002.

[127] G. Vidal, J. I. Latorre, E. Rico, and A. Kitaev, Phys. Rev. Lett. **90**, 227902 (2003).

[128] F. H. L. Essler, S. Kehrein, S. R. Manmana, and N. J. Robinson, Phys. Rev. B **89**, 165104 (2014).

[129] For $J_\perp/J_z$ too small, the linear behavior is contaminated with finite-size effects for the relevant times and system sizes we consider.

[130] C. De Grandi, V. Gritsev, and A. Polkovnikov, Phys. Rev. B **81**, 012303 (2010).

[131] C. De Grandi, V. Gritsev, and A. Polkovnikov, Phys. Rev. B **81**, 224301 (2010).

[132] V. Gritsev and A. Polkovnikov, in *Understanding in Quantum Phase Transitions*, edited by L. Carr (Taylor & Francis, Oxford, UK, 2010).

[133] L. Mathey and A. Polkovnikov, Phys. Rev. A **81**, 033605 (2010).

[134] L. Mathey, K. J. Günter, J. Dalibard, and A. Polkovnikov, arXiv:1112.1204.

[135] A. Mitra and T. Giamarchi, Phys. Rev. Lett. **107**, 150602 (2011).

[136] A. Mitra and T. Giamarchi, Phys. Rev. B **85**, 075117 (2012).

[137] A. Mitra, Phys. Rev. Lett. **109**, 260601 (2012).

[138] R. Vosk and E. Altman, Phys. Rev. Lett. **110**, 067204 (2013).

[139] C. Karrasch, J. Rentrop, D. Schuricht, and V. Meden, Phys. Rev. Lett. **109**, 126406 (2012).

[140] S. D. Sarkar, R. Sensarma, and K. Sengupta, J. Phys.: Condens. Matter **26**, 325602 (2014).

[141] E. G. Dalla Torre, E. Demler, and A. Polkovnikov, Phys. Rev. Lett. **110**, 090404 (2013).

[142] Specifically, ϕ is defined so that its spatial derivative is the fermion density obtained by a Jordan-Wigner transform.

[143] R. Bistritzer and E. Altman, Proc. Natl. Acad. Sci. USA **104**, 9955 (2007).

[144] For $\varphi \neq 0, \pi$ the evolution of S^x corresponds to a decay from dephasing of the individually oscillating excitations. The frequency of the oscillations is approximately given by $\delta J \langle S^z \rangle = \delta J \cos \varphi$. The resulting damped dynamics of $\langle S^x \rangle$ is described by the Luttinger liquid Hamiltonian Eq. (32), with renormalized bosonic density $\rho_0 = (1 - |\cos \varphi|)/(2a)$. Note that the states at $\varphi = 0, \pi$ are exact eigenstates of the XXZ model and consequently do not evolve dynamically.

[145] M. Heyl, A. Polkovnikov, and S. Kehrein, Phys. Rev. Lett. **110**, 135704 (2013).

[146] M. L. Wall and L. D. Carr, Open Source TEBD, 2009, http://physics.mines.edu/downloads/software/tebd

[147] B. Bauer *et al.*, J. Stat. Mech.: Theory Exp. (2011) P05001.

[148] W. Liu and N. Andrei, Phys. Rev. Lett. **112**, 257204 (2014).

[149] M. Takahashi, *Thermodynamics of One-Dimensional Solvable Models* (Cambridge University Press, Cambridge, UK, 1999).

[150] P. Barmettler, M. Punk, V. Gritsev, E. Demler, and E. Altman, New J. Phys. **12**, 055017 (2010).

[151] E. G. Dalla Torre, E. Demler, T. Giamarchi, and E. Altman, Phys. Rev. B **85**, 184302 (2012).

[152] A. Mitra, Phys. Rev. B **87**, 205109 (2013).

[153] I. Bloch, J. Dalibard, and W. Zwerger, Rev. Mod. Phys. **80**, 885 (2008).

[154] F. Pollmann, M. Haque, and B. Dóra, Phys. Rev. B **87**, 041109 (2013).

[155] B. P. Lanyon, C. Hempel, D. Nigg, M. Mller, R. Gerritsma, F. Zhringer, P. Schindler, J. T. Barreiro, M. Rambach, G. Kirchmair, M. Hennrich, P. Zoller, R. Blatt, and C. F. Roos, Science **334**, 57 (2011).

[156] H. Weimer, M. Müller, I. Lesanovsky, P. Zoller, and H. Büchler, Nat. Phys. **6**, 382 (2010).

[157] R. Löw, H. Weimer, J. Nipper, J. Balewski, B. Butscher, H. Büchler, and T. Pfau, J. Phys. B: At. Mol. Opt. Phys. **45**, 113001 (2012).

[158] D. Greif, T. Uehlinger, G. Jotzu, L. Tarruell, and T. Esslinger, Science **340**, 1307 (2013).

[159] J. Simon, W. S. Bakr, M. Ruichao, M. E. Tai, P. M. Preiss, and M. Greiner, Nature (London) **472**, 307 (2011).

[160] S. Prawer and A. D. Greentree, Science **320**, 1601 (2008).

[161] G. Kaur, A. Ajoy, and P. Cappellaro, New J. Phys. **15**, 093035 (2013).

[162] G. A. Álvarez, R. Kaiser, and D. Suter, Ann. Phys. (Berlin) **525**, 833 (2013).

[163] G. A. Álvarez and D. Suter, Phys. Rev. A **84**, 012320 (2011).

[164] G. A. Álvarez and D. Suter, Phys. Rev. Lett. **104**, 230403 (2010).

[165] I. Vragović and R. Scholz, Phys. Rev. B **68**, 155202 (2003).

[166] M. Combescot and W. Pogosov, Phys. Rev. B **77**, 085206 (2008).

[167] M. Litinskaya and R. V. Krems, in *Annual Review of Cold Atoms and Molecules*, Vol. 1, edited by K. W. Madison, Y. Wang, A. M. Rey, and K. Bongs (World Scientific Publishing, Singapore, 2013), Chap. 2.

[168] P. Xiang, M. Litinskaya, and R. V. Krems, Phys. Rev. A **85**, 061401 (2012).

[169] S. Hoyer, F. Caruso, S. Montangero, M. Sarovar, T. Calarco, M. B. Plenio, and K. B. Whaley, New J. Phys. **16**, 045007 (2014).

[170] S. K. Saikin, A. Eisfeld, S. Valleau, and A. Aspuru-Guzik, Nanophotonics **2**, 21 (2013).

[171] A. Micheli, G. K. Brennen, and P. Zoller, Nat. Phys. **2**, 341 (2006).

[172] N. Y. Yao, C. R. Laumann, A. V. Gorshkov, S. D. Bennett, E. Demler, P. Zoller, and M. D. Lukin, Phys. Rev. Lett. **109**, 266804 (2012).

[173] N. Y. Yao, A. V. Gorshkov, C. R. Laumann, A. M. Läuchli, J. Ye, and M. D. Lukin, Phys. Rev. Lett. **110**, 185302 (2013).

[174] J. K. Freericks, M. M. Maśka, A. Hu, T. M. Hanna, C. J. Williams, P. S. Julienne, and R. Lemanski, Phys. Rev. A **81**, 011605 (2010).

[175] A. Chotia, B. Neyenhuis, S. A. Moses, B. Yan, J. P. Covey, M. Foss-Feig, A. M. Rey, D. S. Jin, and J. Ye, Phys. Rev. Lett. **108**, 080405 (2012).

[176] C.-C. Joseph Wang and J. K. Freericks, Phys. Rev. A **86**, 032329 (2012).

[177] B. Huber, T. Baluktsian, M. Schlagmüller, A. Kölle, H. Kübler, R. Löw, and T. Pfau, Phys. Rev. Lett. **107**, 243001 (2011).

[178] T. Baluktsian, B. Huber, R. Löw, and T. Pfau, Phys. Rev. Lett. **110**, 123001 (2013).

[179] R. Löw, H. Weimer, U. Krohn, R. Heidemann, V. Bendkowsky, B. Butscher, H. P. Büchler, and T. Pfau, Phys. Rev. A **80**, 033422 (2009).

[180] W. R. Anderson, J. R. Veale, and T. F. Gallagher, Phys. Rev. Lett. **80**, 249 (1998).

[181] I. Mourachko, D. Comparat, F. de Tomasi, A. Fioretti, P. Nosbaum, V. M. Akulin, and P. Pillet, Phys. Rev. Lett. **80**, 253 (1998).

[182] G. Günter, H. Schempp, M. Robert-de Saint-Vincent, V. Gavryusev, S. Helmrich, C. S. Hofmann, S. Whitlock, and M. Weidemüller, Science **342**, 954 (2013).

[183] J. Stuhler, A. Griesmaier, T. Koch, M. Fattori, T. Pfau, S. Giovanazzi, P. Pedri, and L. Santos, Phys. Rev. Lett. **95**, 150406 (2005).

[184] M. Fattori, T. Koch, S. Goetz, A. Griesmaier, S. Hensler, J. Stuhler, and T. Pfau, Nat. Phys. **2**, 765 (2006).

[185] D. Jaksch, C. Bruder, J. I. Cirac, C. W. Gardiner, and P. Zoller, Phys. Rev. Lett. **81**, 3108 (1998).

[186] M. Greiner, O. Mandel, T. Esslinger, T. W. Hänsch, and I. Bloch, Nature (London) **415**, 39 (2002).

[187] R. Jördens, N. Strohmaier, K. Günter, M. Henning, and T. Esslinger, Nature (London) **455**, 204 (2008).

[188] U. Schneider, L. Hackermüller, S. Will, T. Best, I. Bloch, T. A. Costi, R. W. Helmes, D. Rasch, and A. Rosch, Science **322**, 1520 (2008).

[189] L.-M. Duan, E. Demler, and M. D. Lukin, Phys. Rev. Lett. **91**, 090402 (2003).

[190] C. J. Wu, J. P. Hu, and S. C. Zhang, Phys. Rev. Lett. **91**, 186402 (2003).

[191] A. Gorshkov, M. Hermele, V. Gurarie, C. Xu, P. Julienne, J. Ye, P. Zoller, E. Demler, M. Lukin, and A. Rey, Nat. Phys. **6**, 289 (2010).

[192] M. A. Cazalilla, A. F. Ho, and M. Ueda, New J. Phys. **11**, 103033 (2009).

[193] M. Cazalilla and A. Rey, Rep. Prog. Phys. **77**, 124401 (2014).

[194] S. Stellmer, R. Grimm, and F. Schreck, Phys. Rev. A **84**, 043611 (2011).

[195] S. Taie, R. Yamazaki, S. Sugawa, and Y. Takahashi, Nat. Phys. **8**, 825 (2012).

[196] X. Zhang, M. Bishof, S. L. Bromley, C. V. Kraus, M. S. Safronova, P. Zoller, A. M. Rey, and J. Ye, Science **345**, 1467 (2014).

[197] F. Scazza, C. Hofrichter, M. Höfer, P. C. De Groot, I. Bloch, and S. Fölling, Nat. Phys. **10**, 779 (2014).

[198] S. Sugawa, K. Inaba, S. Taie, R. Yamazaki, M. Yamashita, and Y. Takahashi, Nat. Phys. **7**, 642 (2011).

[199] M. Bishof, M. J. Martin, M. D. Swallows, C. Beno, Y. G. Lin, G. Quemener, A. M. Rey, and J. Ye, Phys. Rev. A **84**, 052716 (2011).

[200] A. D. Ludlow, N. D. Lemke, J. A. Sherman, C. W. Oates, G. Quémener, J. von Stecher, and A. M. Rey, Phys. Rev. A **84**, 052724 (2011).

[201] M. M. Boyd, T. Zelevinsky, A. D. Ludlow, S. M. Foreman, S. Blatt, T. Ido, and J. Ye, Science **314**, 1430 (2006).

[202] G. K. Campbell, M. M. Boyd, J. W. Thomsen, M. J. Martin, S. Blatt, M. D. Swallows, T. L. Nicholson, T. Fortier, C. W. Oates, S. A. Diddams, N. D. Lemke, P. Naidon, P. Julienne, J. Ye, and A. D. Ludlow, Science **324**, 360 (2009).

[203] S. Sachdev, K. Sengupta, and S. M. Girvin, Phys. Rev. B **66**, 075128 (2002).

[204] M. Florian, M. Mark, E. Kirilov, K. Lauber, P. Weinmann, M. Gröbner, A. J. Daley, and H. Nägerl, Science **344**, 1259 (2014).

[205] C. P. Rubbo, S. R. Manmana, B. M. Peden, M. J. Holland, and A. M. Rey, Phys. Rev. A **84**, 033638 (2011).

[206] A. Polkovnikov, Ann. Phys. **325**, 1790 (2010).

[207] W. M. Witzel, R. de Sousa, and S. Das Sarma, Phys. Rev. B **72**, 161306 (2005).

[208] W. M. Witzel and S. Das Sarma, Phys. Rev. B **74**, 035322 (2006).

[209] J. R. Maze, J. M. Taylor, and M. D. Lukin, Phys. Rev. B **78**, 094303 (2008).

[210] K. R. A. Hazzard, A. V. Gorshkov, and A. M. Rey, Phys. Rev. A **84**, 033608 (2011).

[211] T. W. B. Kibble, J. Phys. A: Math. Gen. **9**, 1387 (1976).

[212] W. H. Zurek, Nature (London) **317**, 505 (1985).

[213] D. M. Basko, I. L. Aleiner, and B. L. Altshuler, Ann. Phys. **321**, 1126 (2006).

[214] A. Pal and D. A. Huse, Phys. Rev. B **82**, 174411 (2010).

[215] D. Pekker, G. Refael, E. Altman, E. Demler, and V. Oganesyan, Phys. Rev. X **4**, 011052 (2014).

[216] M. P. Kwasigroch and N. R. Cooper, Phys. Rev. A **90**, 021605(R) (2014).

[217] N. Y. Yao, C. R. Laumann, S. Gopalakrishnan, M. Knap, M. Mueller, E. A. Demler, and M. D. Lukin, arXiv:1311.7151.